Ecological Indicators 171 (2025) 113211

Contents lists available at ScienceDirect

Ecological Indicators

journal homepage: www.elsevier.com/locate/ecolind

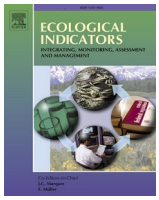

Assessing sargassum pressure on coastal habitats using a spatial and temporal approach at the territorial scale

Mathilde Teyssier [a,b,*], Catherine Desrosiers [a], Claire Hellio [b], Fanny Kerninon [b]

[a] Impact Mer, 20 rue Karukera, F-97200 Fort-de-France, Martinique, France
[b] Univ Brest, CNRS, IRD, Ifremer, LEMAR, F-29280 Plouzané, France

ARTICLE INFO

Keywords:
Sargassum influxes
Pressure indicators
Monitoring
Territorial scale
Management
Mangroves
Seagrass meadows

ABSTRACT

Since 2011, coastal areas of the Caribbean Sea and the Tropical Atlantic Ocean have been exposed to massive influxes of pelagic sargassum algae. Coastal sargassum accumulations and brown water associated with their decomposition represent a new pressure threatening ecosystems, human health and the socio-economic sector. There is still a lack of well-calibrated monitoring methods to accurately characterise sargassum pressure at the scale of a territory. This study aimed to develop a methodology for quantifying, locating, and monitoring the dynamics of sargassum pressure on Martinique's coastal environment (Lesser Antilles). Monthly aerial monitoring and daily records of *in situ* cameras were used to develop pressure indicators for sargassum accumulations and brown water. Thanks to these indicators, we identified the areas most exposed to sargassum pressure: the innermost parts of the bays characterised by low hydrodynamic conditions, particularly the mangroves, and very exposed to prevailing winds. In these areas, dense accumulations persist all over the year, even during lulls in sargassum influxes. Coastal marine habitats, such as seagrass meadows, are mainly exposed to brown water, particularly during heavy rainfall, which causes brown water to spread offshore. Our methodology has proved to be an effective tool for territorial diagnosis, enabling the identification of sites at stake and periods at risk. It provided a better understanding of spatial variations and drivers of exposure to three different decomposition states of sargassum (stranded, stagnant and brown water). These data are invaluable to managers, researchers, and entrepreneurs and can be helpful to other regions that are exposed to sargassum influxes as part of health, socio-economic, or environmental impact studies.

1. Introduction

Since 2011, massive influxes of holopelagic sargassum species (*Sargassum natans* and *Sargassum fluitans*) have reached the coasts of the Caribbean, the Gulf of Mexico and West Africa (Gower et al., 2013). These influxes originate from a new source region outside the Sargasso Sea, the North Equatorial Recirculation Region (NERR) (Franks et al., 2016). In this region, sargassum rafts follow the seasonal migration of the Inter-Tropical Convergence Zone (ITCZ) (Johns et al., 2020). In summer, sargassum algae expand both westward and eastward, forming the Great Atlantic Sargassum Belt (GASB) (Wang et al., 2019). While the ocean circulation mainly drives the distribution of sargassum, the occurrence of a bloom leading to massive influxes could be explained by several drivers (Marsh et al., 2023), such as the Atlantic Meridional Mode and the Atlantic Niño (Skliris et al., 2022), sea surface temperature patterns, (Wang et al., 2019), and nutrient availability through discharges from large rivers such as the Amazon (Lapointe et al., 2021), upwellings in the open ocean and along the coast of African, hurricanes (Oviatt et al., 2019) and possibly Saharan dust (Wang and Hu, 2016). The multiplicity of basin-scale drivers explains the great interannual variability in sargassum influx intensity since 2011 (Wang et al., 2019; Skliris et al., 2022). The accumulation and decomposition of large amounts of sargassum along the shoreline have significant negative impacts on human health and well-being (Resiere et al., 2018; Mendez-Tejeda et al., 2019), socio-economic sectors such as tourism and fisheries (Solarin et al., 2014; UNEP-CEP, 2021), and coastal ecosystems (van Tussenbroek et al., 2017; Rodríguez-Martínez et al., 2019). It has become a serious concern for public policy-makers and stakeholders in the affected territories (UNEP-CEP, 2021).

Forecasting and monitoring data on sargassum influxes are essential for anticipating and adapting local management actions. The scientific research effort on this topic has significantly increased over the last

* Corresponding author at: Impact Mer, 20 rue Karukera, F-97200 Fort-de-France, Martinique, France.
E-mail address: mteyssier@impact-mer.fr (M. Teyssier).

https://doi.org/10.1016/j.ecolind.2025.113211
Received 15 October 2024; Received in revised form 5 February 2025; Accepted 6 February 2025
Available online 14 February 2025

decade (Fidai et al., 2020). Forecasting sargassum influxes relies heavily on satellite imagery to detect sargassum in the Atlantic Ocean (Maréchal et al., 2017; Arellano-Verdejo et al., 2022). Several forecasting bulletins are now accessible online, such as the Sargassum Outlook Bulletin of the University of South Florida (USF), the Sargassum Inundation Risk (SIR) developed by the National Oceanic and Atmospheric Administration (NOAA) and the USF, the Sub-Regional Outlook Bulletin of UWI-CERMES (Centre for Resource Management and Environmental Studies), and the forecast bulletin of Météo France, the official French meteorological administration. Monitoring sargassum influxes along the coast relies on various methodologies presented in the scientific literature. Some are based on satellite data, such as the methodology developed by León-Pérez et al. (2023), using the Random Forest model combined with Sentinel-2. Their algorithm enables the differentiation of fresh sargassum, decomposing sargassum and brown water resulting from decomposition along the shoreline (10 m resolution). Other methodologies involve data collected *in situ*. Some studies use data from participatory science and crowdsourcing initiatives to estimate the level of accumulation of stranded sargassum based on photos taken by a network of volunteers (Arellano-Verdejo and Lazcano-Hernández, 2021). This estimation can be carried out by eye, as demonstrated in the Sargassum Watch project (Iporac et al., 2022). Four classes established by Collado-Vides et al. (2018) are used to estimate the quantity of stranded sargassum visualised in the photos. Image analysis can also be performed using artificial intelligence (AI) algorithms, such as convolutional neural networks (CNN) used in the "Collective View" application (Arellano-Verdejo and Lazcano-Hernández, 2021), or through semantic segmentation (SS) (Arellano-Verdejo et al., 2022). These algorithms automatically classify each image pixel into categories such as sargassum, sea, beach, vegetation, etc. Other studies have monitored sargassum stranding dynamics along the coast using *in situ* cameras. The area covered by stranded sargassum is determined by AI with Machine Learning (Rutten et al., 2021) and Deep Learning (Valentini and Balouin, 2020; Uribe-Martinez et al., 2022).

While these methods are helpful in quantifying sargassum accumulations across both the Atlantic Ocean and coastal regions, they have several limitations. Satellite detection of sargassum can be affected by various factors, including atmospheric humidity, clouds, solar radiation, water depth, turbidity and sand haze (Wang and Hu, 2016). According to the sensor resolution, the pixel size may not accurately measure the area covered by sargassum (Hu et al., 2021). These biases can lead to disparities between the biomass estimated by satellite and that encountered on beaches (Rodríguez-Martínez et al., 2022). Higher resolution can improve the accuracy of the measured area, such as with Sentinel-2 (10 m resolution) and the new generation of Dove satellites (3 m resolution). Nevertheless, it is still insufficient to determine the depth and, consequently, the volume of sargassum accumulations. The volume can vary significantly due to the great variability in raft shape, size and thickness at sea, and on the coast, where sargassum accumulations form thick mats (Ody et al., 2019). The same problem applies to camera data. The area covered by sargassum is reported without considering the density of the biomass. Currently, limited scientific publications estimate the volume of stranded or potentially stranded sargassum and calculation methods vary (Fidai et al., 2020). For example, Rodríguez-Martínez et al. (2022) used hotel beach cleaning data to estimate volumes of stranded sargassum. These data are limited to a number of sites, and volumes can be overestimated as reported volumes can also include sand and seagrass debris. The protocol proposed by Baldwin et al. (2022), linking image acquisition by unmanned aerial vehicles with *in situ* biomass measurements, is suitable for a station-based study. However, it does not allow for quantifying strandings at the scale of a territory. Finally, participatory data collection tools provide a large but sporadic dataset of accumulation levels (Arellano-Verdejo and Lazcano-Hernández, 2021).

Our study aimed to develop a more accurate method to evaluate the pressure of sargassum on the coastal environment while working on the scale of Martinique (Lesser Antilles). Aerial and *in situ* camera monitoring programmes were conducted to collect data that we used to design pressure indicators on different spatial and temporal scales. The developed indicators were compared with other data to test their robustness and usefulness for public policies and local authorities. The study focused on the level of exposure to sargassum pressure in coastal marine habitats, such as mangroves, seagrass meadows, and coral reefs, due to the important ecosystem services they provide for the region (Barbier et al., 2011).

2. Materials and methods

2.1. Terminology used in this study

The terms used in this manuscript are defined in Table 1.

2.2. Study area

The study was conducted in Martinique, a French Caribbean island in the Lesser Antilles (Fig. 1). Its tropical climate depends on the Azores anticyclone and the Inter-Tropical Convergence Zone (ITCZ). It is characterised by a dry season, from February to April and a wet season, from July to October. Dry and wet seasons are separated by two relatively distinct inter-seasonal periods. The North Equatorial Current (NEC) and the North Brazilian Current (NBC) influence the Lesser Antilles. The NEC induces a westerly to southwesterly flow off Martinique (Actimar, 2020). The NBC retroflexion causes large anticyclonic eddies, which episodically reach the south of the Lesser Antilles. The wind regime is characterised by the northeast trade winds, which flow in the same direction as the Atlantic currents. This means that prevailing winds affecting Martinique come from the northeast, east and southeast. On the Atlantic coast of Martinique, the surface current flows predominantly from south to north. It bifurcates in the southern part of the island with a northwesterly branch. Tidal currents are generally weak and have minimal impact on surface circulation. The deep current is similar to the surface current. Swells mainly come from the north, northeast and east (Pujos et al., 1992). Therefore, sargassum rafts come

Table 1
Terminology used in this manuscript.

Term	Definition
sargassum:	holopelagic brown algae of the genus *Sargassum* (C. Agardh, 1820) (*S. fluitans, S. natans*)
sargassum raft:	a floating mass of drifting sargassum
sargassum influx:	arrival of sargassum rafts in coastal areas
sargassum stranding:	a phenomenon where sargassum washes ashore and becomes deposited on beaches or onshore areas
stranded sargassum:	sargassum that has been deposited onshore
stagnant sargassum:	sargassum that remains stationary in the water due to accumulation along the coast or behind an obstacle. While it may still be floating (particularly the upper part), it is often submerged due to the accumulation of successive arrivals and ongoing decomposition.
sargassum accumulation:	gathering of sargassum at the coast or behind an obstacle, either on land in the case of stranded sargassum or in the water in the case of stagnant sargassum
brown water:	leachates and organic particles from sargassum decomposition
sargassum brown tide:	initially introduced by van Tussenbroek et al. (2017), this phenomenon is interpreted here as a massive accumulation of holopelagic sargassum along the coast accompanied by a discharge of brown water, which has a negative connotation.
sargassum feature:	spatial entity associated with sargassum decomposition states (stranded, stagnant or brown water), typically represented as a polygon in a geographic information system (GIS)
sargassum pressure:	direct stress exerted by sargassum (stranded, stagnant and/or brown water) on the environment or individuals, which may lead to potential impacts

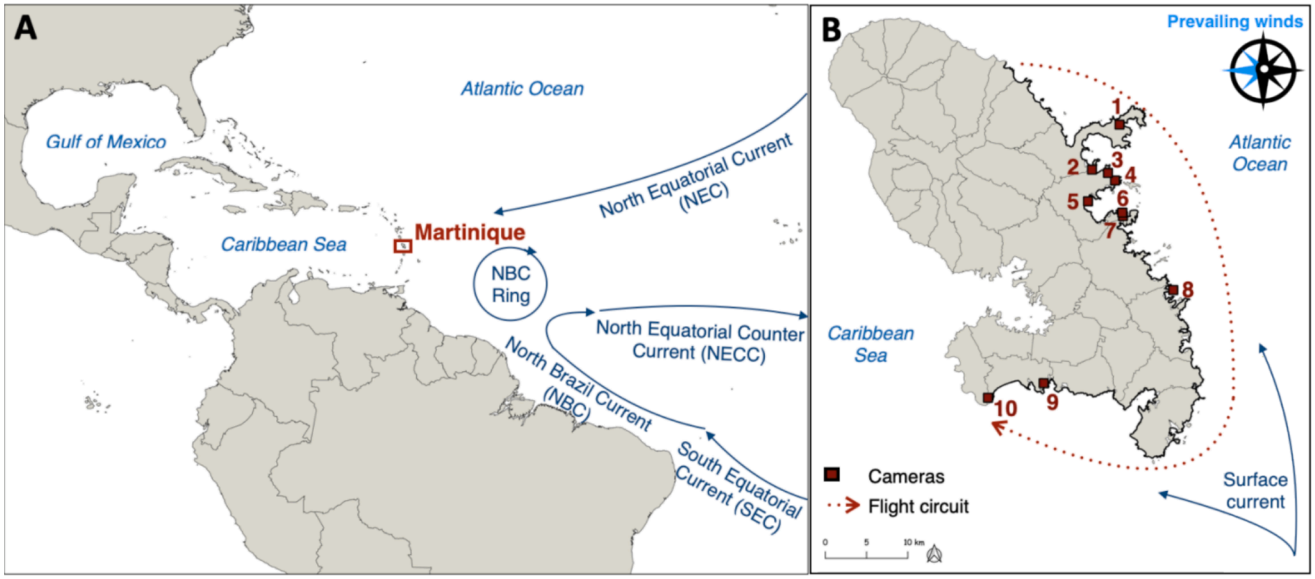

Fig. 1. Location of Martinique in the Caribbean Sea (A), aerially monitored coastline and locations of *in situ* monitored cameras (B). Site 1: Trésor, Site 2: Galion, Site 3: Cayol, Site 4: Barrier of Cayol, Site 5: Bourg du Robert, Site 6: Pointe Hyacinthe, Site 7: Sable blanc, Site 8: Barrier of Cap Est, Site 9: Taupinière, Site 10: Anse Caffard. Base maps: World Country Polygons VHR – World Bank Group (A), BD TOPO® 2019 – IGN (National Institute for Geographic and Forestry Information) (B).

from the Atlantic Ocean, driven by the NEC, NBC, and trade winds, and mainly affect the Atlantic and south coasts of Martinique. The precise location of coastal sargassum accumulations is challenging to predict due to geometry of the coast and associated local hydrodynamics, which remain poorly documented due to the lack of small-scale studies.

2.3. Monitoring strategy

Two complementary monitoring programmes were conducted to characterise the intensity, location, and frequency of sargassum influxes and related pressure along the coast of Martinique.

The purpose of the aerial monitoring was to locate and quantify sargassum pressure along the entire exposed coastline of Martinique (Fig. 1). The monitoring was conducted monthly via gyrocopter flights between May 2022 and December 2023. During each of the 20 flights, every section of the shoreline with sargassum accumulations and brown water was photographed. In contrast to unmanned aerial vehicles, this approach allows for the observation at a very high resolution of an entire territory. This method is the first to quantify sargassum accumulations at this scale. Preliminary work was carried out by the DEAL Martinique (Direction de l'Environnement, de l'Aménagement et du Logement de la Martinique), a department of the French Ministry of Environment, using a rotorcraft to characterise massive influxes in 2018 and 2019. In addition, the CEVA (Centre d'Étude et de Valorisation des Algues / algae technology and innovation centre) has conducted airborne monitoring for several years to characterise green tides of *Ulva* algae in Brittany (France), which is similar in some ways to sargassum brown tides.

The *in situ* camera monitoring aimed to determine the dynamics of sargassum influxes and associated pressure at a site scale. Daily observations of ten cameras were conducted between January 2022 and December 2023 (Fig. 1). The system, described by Valentini and Balouin (2020), comprises smartphone cameras (SOLARCAM ©), autonomous thanks to a solar panel. The cameras have a resolution of 12 million pixels and are set to take one photo per hour between 7 a.m. and 5 p.m. They are user-friendly, affordable, and provide real-time image viewing on a dedicated website. We chose this system because it was successfully used for a previous morphodynamics and sargassum monitoring programme in Martinique (Bouvier, 2024). The study sites were selected in collaboration with territorial managers for their ecological interest and to represent presumed differences in sargassum pressure, with a diversity of bay exposure and hydrodynamics (Fig. 2). The calculation of the bay exposure is illustrated for "Trésor" (site 1). It represents the opening angle through which sargassum rafts can reach the site by drifting with the prevailing winds. Hydrodynamic conditions are determined based on field observations. This monitoring approach is complementary to aerial monitoring, as it takes account of accumulation dynamics associated with environmental conditions. The study of accumulation dynamics includes exposure time in characterising sargassum pressure, while aerial monitoring provides a snapshot of the situation at a given time.

2.4. Indicators of sargassum pressure

The methodology described in the following sections and illustrated in a flowchart (Fig. 3) was validated by the statistical analyses presented in paragraph 2.5.1.

Firstly, a grid covering the entire coastal environment of Martinique with a cell area equivalent to 100,000 m^2 was created in QGIS (see Fig. 2). Each coastal cell was cut to only include areas likely to be affected by sargassum (sea and foreshore). Some cells were then merged and recut to ensure a minimum of 100,000 m^2. This grid made it possible to consider comparable geographical features and consequently identify which sites (cells) are the most exposed to sargassum pressure. The objective was to determine sargassum pressure inside each coastal cell of the grid. Aerial monitoring provided data for quantifying sargassum pressure in all coastal cells once a month. *In situ* camera monitoring provided data to quantify sargassum pressure in the cell corresponding to the camera's field of view at each study site daily (Fig. 2).

2.4.1. Frequency of sargassum influxes (F_{sarg})

The quantity of sargassum accumulated on the coast depends on the frequency and intensity of sargassum influxes. Daily *in situ* camera observations enabled us to monitor sargassum influxes. Each day, the presence/absence of a new influx at each study site was reported in a database. In the event of a new influx, the intensity was visually estimated using four classes (Fig. 4). For each site, the monthly frequency of influxes (F_{sarg}) was calculated by dividing the number of days with a new influx by the total number of days monitored monthly.

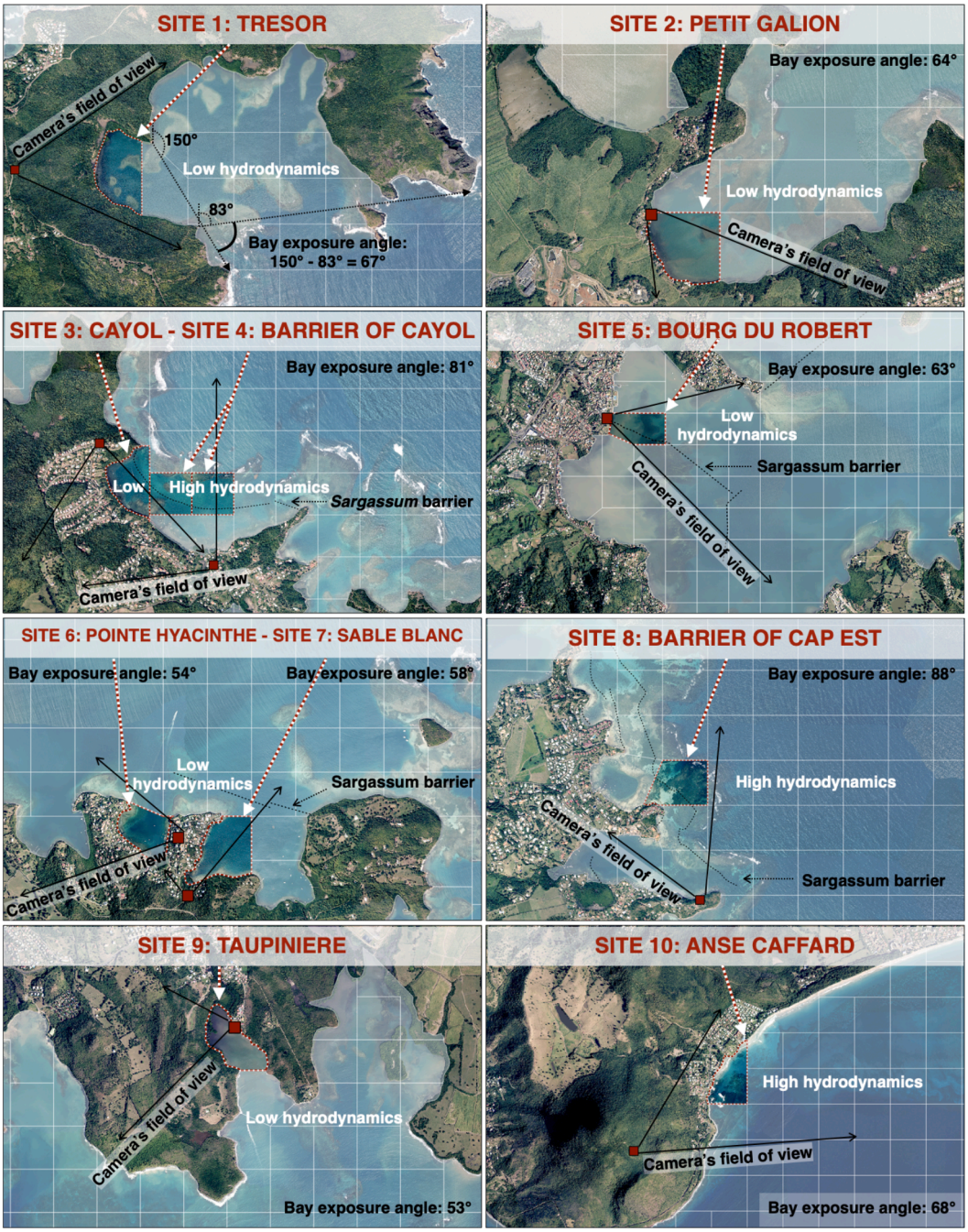

Fig. 2. Sites monitored by *in situ* cameras. The study area of each site is defined by a cell within a grid that encompasses the entire coastal zone of Martinique. The dimensions of each grid cell are 100,000 m^2, with the exception of the recut coastal cells, which may possess a larger area. In the site Barrier of Cayol (4), two cells are considered due to the observed drift of sargassum accumulations along the sargassum barrier. Base map: ORTHO HR® 2017 – IGN.

2.4.2. Sargassum area

We estimated the sargassum surface area during both monitoring surveys, where sargassum features were classified as stranded, stagnant, or brown water (Appendix A, Fig. A.1).

2.4.2.1. Aerial monitoring. For all 20 flights, every sargassum feature visible along the coastline in the aerial photographs was digitised using QGIS. The ORTHO HR® 2017 from the IGN (National Institute for Geographic and Forestry Information) was used as the reference layer. The digitisation process used raw photographs instead of georeferenced ones because the lengthy georeferencing process would have been impractical for an average of 500 photos per flight. Therefore, the boundaries of sargassum features were visually transferred from the raw aerial photographs to the ORTHO HR® in QGIS using a multitude of visual reference points, including the coastline, residential structures, pontoons, reefs, seabed, and other pertinent features (Appendix A, Fig. A.2). The area of each sargassum feature (polygon) was then calculated.

2.4.2.2. In situ camera monitoring. The cameras were programmed to capture one photograph per hour between 7 a.m. and 5 p.m., resulting in a total of 11 photographs per day. This equates to nearly 8,000 photographs per site throughout the two-year study period. The quantity of data did not allow the digitisation of sargassum features observed in the time-lapse images of each camera in QGIS. Consequently, the area of stagnant sargassum and brown water was visually estimated each day by

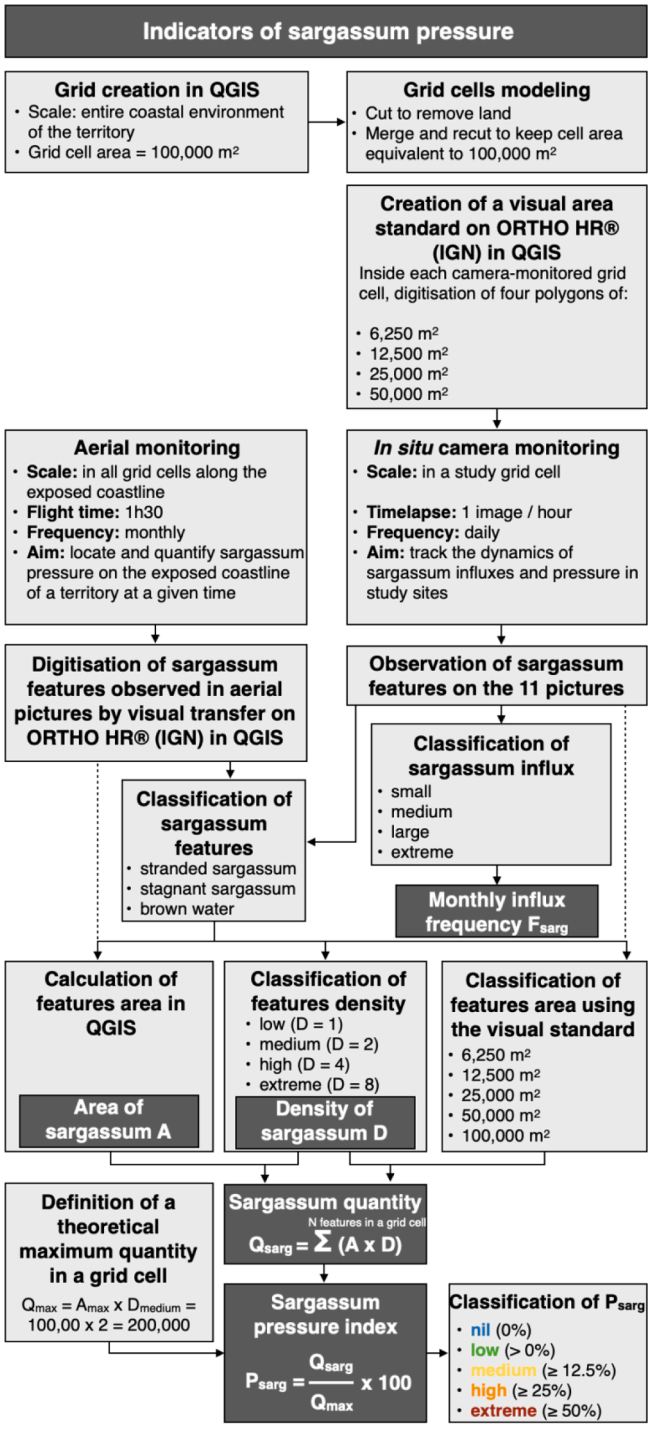

Fig. 3. Methodological flowchart of the development of sargassum pressure indicators.

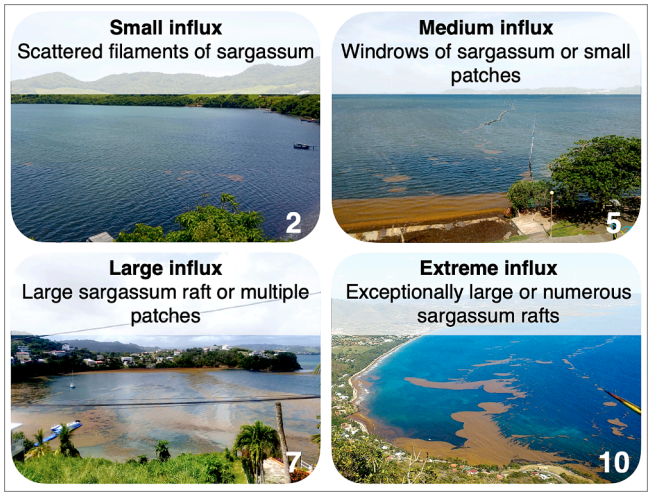

Fig. 4. Classes used to evaluate the intensity of sargassum influxes with an example at four *in situ* camera-monitored sites (2, 5, 7, 10). Inspired by Ody et al. (2019).

Table 2
Classes of sargassum area estimated during the land-based camera monitoring.

Estimated range area (A)	Recorded area
$0 < A < 6{,}250\ m^2$	$6{,}250\ m^2$
$6{,}250\ m^2 \leq A < 12{,}500\ m^2$	$12{,}500\ m^2$
$12{,}500\ m^2 \leq A < 25{,}000\ m^2$	$25{,}000\ m^2$
$25{,}000\ m^2 \leq A < 50{,}000\ m^2$	$50{,}000\ m^2$
$\geq 50{,}000\ m^2$	$100{,}000\ m^2$

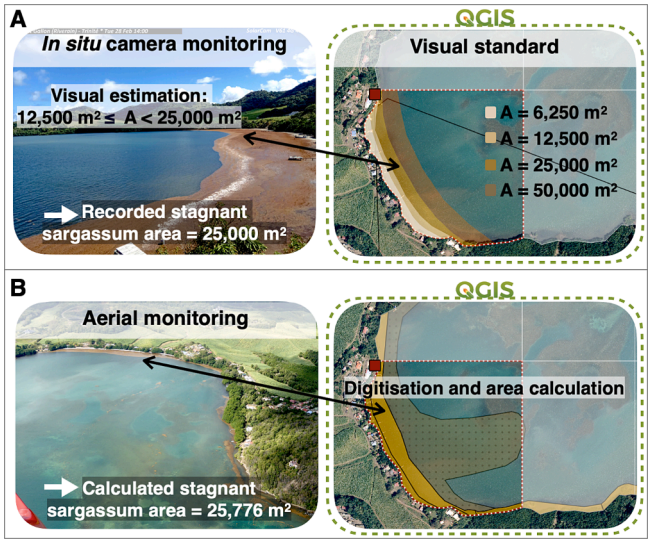

Fig. 5. Example of area determination of stagnant sargassum by camera in Petit Galion (site 2) on February 28, 2023 (A) and comparison with the area calculated from the digitised features during the aerial monitoring the same day (B).

comparing the visual observations in each photograph to five predefined classes digitised in QGIS (Table 2). These classes were digitised in each camera-monitored grid cell using the ORTHO HR® 2017 from IGN (Fig. 5). The digitised classes correspond to the most frequently encountered layout of sargassum accumulations. They were created before the study monitoring period and serve as a visual standard. Since the recorded area corresponds to the upper limit of the estimated range, the visual estimate of the area is overestimated (Table 2). Between each successive class, the area increases by a factor of two until it reaches the theoretical maximum area of the study cell, which is 100,000 m^2 (Fig. 2). The maximum class is 100,000 m^2 (cell area), as this is the largest sargassum feature measured in our data. The class size doubles from one class to the next to ensure consistency with the density scores explained in the following section. The class "6,250 m^2," was added to ensure that small areas observed by the camera *in situ* correspond more closely to those obtained during aerial surveys. After reviewing the 11 photographs per day, the area range was determined using key visual reference points, such as pontoons. In the event of a sargassum influx, the visually estimated area was recorded once the sargassum raft had

accumulated on the shore. The detected area was recorded daily in a database for each site. Of all the sites monitored by cameras, only Anse Caffard (site 10) has a beach where sargassum can strand. The other sites consisted of mangrove areas, urbanised zones or sargassum barriers, where the potential stranding zones were very limited or non-existent, which is also the case for many accumulation zones across Martinique. Therefore, the surface area of stranded sargassum was only estimated for site 10. As the beach is around 3,000 m^2 at this site (i.e. half the area used as the upper limit of the first class), the area of stranded sargassum recorded was always 6,250 m^2.

2.4.3. *Sargassum density*

For each sargassum feature, the density of stranded and stagnant sargassum was visually estimated using four classes and associated scores (Fig. 6) in both the aerial and *in situ* camera monitoring surveys. The density classes involve finding a compromise between acquisition time and data accuracy. Visual estimation has some subjectivity, but distinct classes have been created to minimise this. To determine the score of each class, sargassum surface area captured by a camera before and after it reached the coast was measured (Appendix, Fig. A.3). The area of the sargassum raft decreased by half as it accumulated on the coast. The quantity of sargassum remained constant as the raft approached and accumulated on the coast, doubling the density. As a result, the density score doubles from one class to the next. For brown water, the density score was set at 0.3. This choice is explained below. Although field measurements were planned to assess the reliability of our density estimations, we could not carry them out due to technical constraints.

2.4.4. *Sargassum quantity (Q_{sarg}) and sargassum pressure index (P_{sarg})*

The quantity of sargassum in each polygon was determined by multiplying the area by the density score. The total quantity of sargassum in each grid cell (Q_{sarg}) was calculated by summing the quantity of all sargassum features (polygons) contained in the cell (stranded, stagnant, and brown water) (Fig. 7). A sargassum pressure index (P_{sarg}) was developed to improve the interpretability of the values by dividing the total quantity within a grid cell by a theoretical maximum quantity. According to our observations, the theoretical maximum quantity was set at 200,000, corresponding to a cell containing 100,000 m^2 of stagnant sargassum with a medium density (score = 2). The sargassum pressure index was distributed between five classes for better visual assessment (Table 3, Fig. 8), set to match observations in the field. The density of brown water was set to 0.3 so that a 100,000 m^2 surface area covered with brown water would have a P_{sarg} value of 15% (100,000 x 0.3 / 200,000 x 100), placing it in the medium class. We

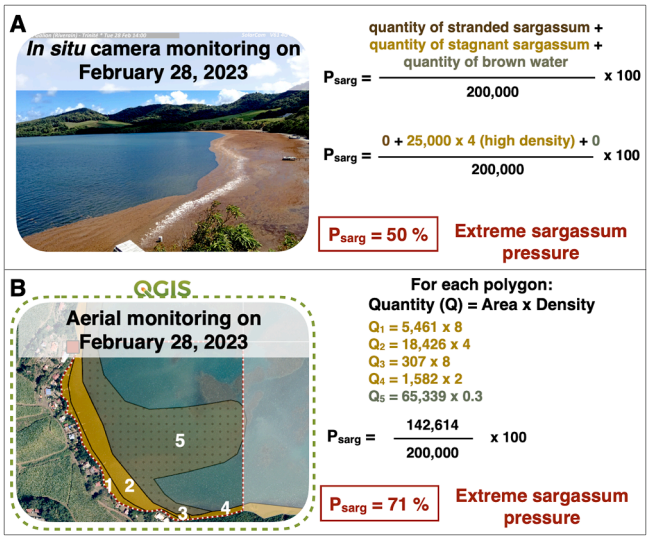

Fig. 7. Example of calculation of the sargassum pressure index (P_{sarg}) from camera time-lapse (A) and from the digitized features of the flight (B) in the grid cell of Petit Galion (site 2) on February 28, 2023.

Table 3
Sargassum pressure index (P_{sarg}) classes.

P_{sarg} (%)	Sargassum pressure
0	Nil
$0 < P_{sarg} < 12,5$	Low
$12,5 \leq Psarg < 25$	Medium
$25 \leq P_{sarg} < 50$	High
≥ 50	Extreme

determined that a grid cell fully covered by brown water, without stranded or stagnant sargassum, would correspond to medium pressure. Such cells are typically located farther offshore, where brown water is more diluted than closer to the shore. This results in lower pressure than a grid cell covered by stagnant sargassum. This is consistent, as brown water represents a much smaller volume of organic material per unit area than sargassum accumulations. We chose 15% to leave enough margin to account for grid cells exceeding 100,000 m^2 (which can happen with modified coastal cells; see Fig. 2). This ensures the pressure index does not shift into the high-pressure class. The potential area of stranded sargassum is much smaller than that of stagnant sargassum or

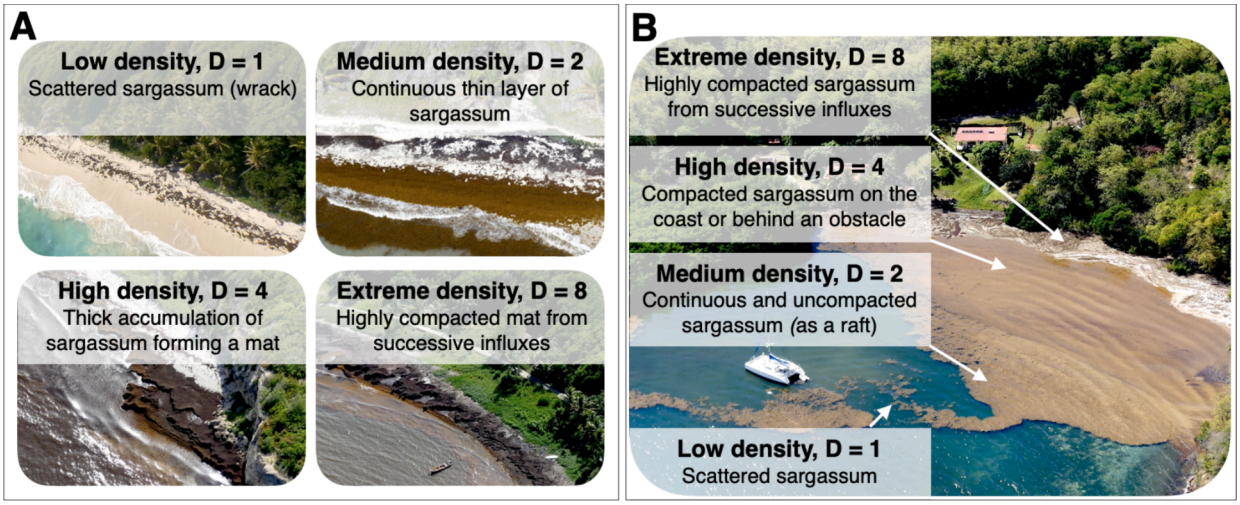

Fig. 6. Classes of density and associated scores (D) for stranded (A) and stagnant (B) sargassum.

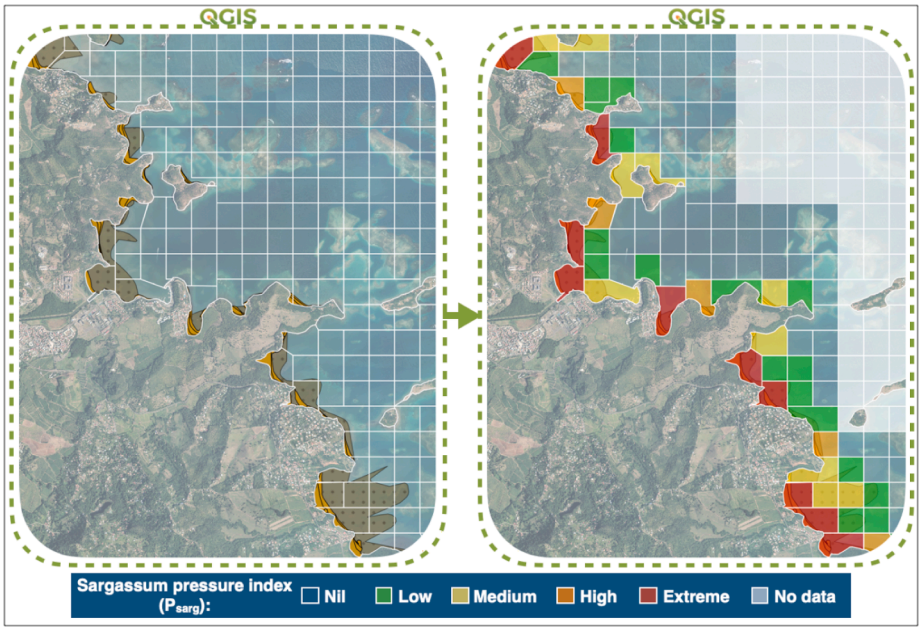

Fig. 8. Example of calculation of the sargassum pressure index (P_{sarg}) in all coastal cells from the digitised features of the 10th flight (February 28, 2023), with a focus on the municipality of Le François.

brown water. Therefore, the total quantity of sargassum (Q_{sarg}) and the pressure index (P_{sarg}) are primarily driven by the area and density of stagnant sargassum. For the calculation of P_{sarg} (Fig. 7), we obtained a difference of 21% between P_{sarg} values from the two monitoring methods. However, the sargassum pressure was classified in the same category (extreme). This difference can be attributed to *in situ* camera monitoring limitations, which provide less precise values than aerial monitoring. Visually estimating surface areas is inherently qualitative, with only five possible values. The recorded density represents the predominant value, and variations of density within accumulations are not accounted for, in contrast to digitised sargassum features from aerial monitoring. In addition, brown water may be difficult to detect, depending on light conditions and the camera's field of view.

2.5. Data analysis

All spatial analyses were performed using QGIS (version LTR 3.34.5) from the QGIS project (QGIS.org, 2024), and all statistical analyses were conducted in RStudio (version 2024.04.1+748) from the R Core Team (2024).

2.5.1. Validation tests

2.5.1.1. Digitisation from raw images vs georeferenced images. The digitisation process used raw aerial photographs instead of georeferenced ones (Appendix A, Fig. A.2). For consistency, we made sure that the two methods were statistically comparable. Thirty images among the 20 flights were randomly selected and georeferenced in QGIS. For georeferencing, 15 to 25 control points, a projective transformation algorithm and a nearest neighbour resampling were used. Sargassum features were digitised from the georeferenced images. The difference between the total area of polygons digitised from the raw images and the one digitised from the georeferenced images was calculated for each image and each sargassum state. The bias corresponds to the mean of differences. A Passing-Bablok regression (Passing and Bablok, 1983), suitable for non-parametric data, was then conducted. The Passing-Bablok line of best-fit ($y = b \times x + a$) and its confidence interval (CI) were calculated by using the "mcreg" function from the "mcr" package (Potapov et al., 2023). If 1 is within the confidence interval of the gradient (b) and 0 within the confidence interval of the y-intercept (a), the two methods are comparable within a 95% confidence interval.

2.5.1.2. Aerial monitoring method vs in situ camera monitoring method for calculating the sargassum pressure index (P_{sarg}). The area of sargassum features is a quantitative variable in the aerial monitoring method, whereas it is a categorical variable in the *in situ* camera monitoring method (Fig. 5). Given this difference in precision, we verified that the *in situ* camera monitoring and the aerial monitoring were statistically comparable for calculating the sargassum pressure index P_{sarg}. As in Fig. 7, we compared P_{sarg} values derived from aerial monitoring (P_{sarg}_flight) and those derived from *in situ* camera monitoring (P_{sarg}_cam) on the day of each of the 20 flights. This comparison was made for all *in situ* camera-monitored sites. The bias or mean of differences between P_{sarg}_flight and P_{sarg}_cam was calculated and a Passing-Bablok regression was performed.

2.5.2. Difference in dynamics of sargassum influxes and pressure index between sites

We hypothesised that exposure to sargassum influxes (F_{sarg}) and pressure (P_{sarg}) depends on the bay exposure angle and hydrodynamic conditions of the site. Study sites were selected to present differences in these two variables (Fig. 2). We tested this hypothesis by performing a Factor Analysis of Mixed Data (FAMD) using the "FAMD" function in the "FactoMineR" package (Le et al., 2008).

2.5.3. Seasonal dynamics of sargassum influxes and associated pressure at the scale of Martinique

The monthly influx frequency at Martinique's scale was calculated by averaging the frequencies of all the *in situ* camera-monitored sites, for each category of influx intensity (small, medium, large, extreme). The same was done for the sargassum pressure index. These two variables were compared with the external data presented in Table 4. The aim was to find a link between the sargassum biomass in the Central Atlantic Ocean, the forecast models, and the influxes observed in Martinique. Monthly precipitation was also taken into account to study its role in sargassum pressure dispersion. The linear relationship between our variables (F_{sarg}, P_{sarg}) and external variables (Table 4) was tested by constructing a correlation matrix using Spearman's test in the "corrplot"

Table 4
External variables compared with our data.

Variables	Source of data	Description
Biomass USF	USF https://optics.marine.usf.edu/projects/saws.html	Monthly sargassum biomass (million tons) in the Central Atlantic Ocean (including the Caribbean Sea and the Gulf of Mexico) from the Sargassum Outlook Bulletin, estimated by satellite data (7-day Floating Algae index)
Risk MF	Météo France https://meteofrance.mq/fr/sargasses	Risk of influx of the 4-day forecast bulletin (1: low, 2: medium, 3: high, 4: very high) on three coastal zones: North Atlantic, South Atlantic, South coast
Risk NOAA/USF	NOAA/USF https://cwcgom.aoml.noaa.gov/SIR/	Weekly Sargassum Inundation Risk (1: low, 2: medium, 3: high) on coastal zones of Martinique using the Alternative Floating Algae Index values in the neighbourhood (50 km) of each coastal pixel.
Precipitation	Météo France https://meteo.data.gouv.fr	Monthly precipitation (mm) was calculated using open access data from Météo France (basic climatological data – decadal agro). A Martinique-wide average was calculated taking into account weather stations located on the south and Atlantic coasts.

package (Wei and Simko, 2021). The comparison between our data and external data also allowed us to test the robustness of the methodology developed.

2.5.4. Exposure of coastal marine communities to sargassum

We calculated the total surface area exposed to sargassum for each of the 20 flights for every coastal marine community using QGIS and Martinique's 2023 coastal marine habitats layer (Nicet, 2024) provided by the French Biodiversity Agency. In addition, the total coastal length of mangroves exposed to sargassum during each flight was determined using the 2019 land use layer (OCS GE) provided by GéoMartinique and IGN. Exposure was categorised into brown water, stagnant sargassum by density class, stagnant sargassum all densities combined, and sargassum across all states combined. The maximum area or length exposed to sargassum across the 20 flights was selected for each category. Finally, the maximum exposure across all states was compared to the total surface area of each marine community and the total coastal length of mangroves in Martinique.

3. Results

3.1. Validation tests of the methodology

3.1.1. Digitisation from raw images vs georeferenced images

The mean percentage difference between the area of total sargassum measured by the "raw method" and that measured by the "georef method" is close to 0 (Table 5). For stranded and stagnant sargassum and brown water, 1 is within the confidence interval (between Upper CI and Lower CI) of the gradient (b), and 0 is within the confidence interval of the y-intercept (a) (Fig. 9). Thus, Passing-Bablok regression indicates that the "raw method" and the "georef method" for measuring the sargassum area are comparable within a 95% confidence interval, regardless of the sargassum state.

3.1.2. Aerial monitoring method vs in situ camera monitoring method to calculate the sargassum pressure index (P_{sarg})

The bias between P_{sarg} values from the aerial monitoring method and P_{sarg} values from the *in situ* camera monitoring method equals 0.69, which is negligible. 1 is within the confidence interval of the gradient, and 0 is within the confidence interval of the y-intercept of the Passing-Bablok equation (Fig. 10). Accordingly, the two methods are comparable for calculating the sargassum pressure index.

Table 5
Bias of the digitisation from raw images compared to the digitisation from georeferenced images. Bias represents the mean of differences expressed in m^2 and percentage. Standard deviations are indicated (± SD).

Sargassum	Difference (m^2)	Percentage difference (%)
stranded	−108 ± 348	− 3.9 ± 27.4
stagnant	−181 ± 2,466	− 2.1 ± 12.8
brown water	+3,338 ± 16,049	+4.3 ± 12.9
Total	**+1,061 ± 9,460**	**−0.2 ± 16.3**

3.2. Location of sites most exposed to sargassum pressure along the coast of Martinique

The aerial monitoring provided a monthly snapshot of sargassum pressure along the coast from May 2022 to December 2023 (20 flights in total) (Appendix A, Fig. A.4). The sargassum pressure index allowed for easy identification of high-risk areas at the island scale on each map. The mean value of P_{sarg} over the 20 flights identified the most exposed sites to sargassum pressure, i.e., those with the highest mean quantities of sargassum along the coast of Martinique surveyed in this study (Fig. 11). Grid cells with high and extreme mean pressure ($P_{sarg} \geq 25\%$), 23 in total, are located in the innermost part of the bays. They are characterised by low hydrodynamic conditions, most of which (20/23) feature mangrove habitats. Twenty-one sites are exposed to northeast wind and 22 to easterly wind.

3.3. Difference in dynamics of sargassum influxes and pressure index between sites

The *in situ* camera monitoring was used to record the occurrence and intensity of sargassum influxes and to calculate the sargassum pressure index (P_{sarg}) daily at each site (Appendix A, Fig. A.5).

Sites monitored by *in situ* cameras were exposed to influxes that varied from one another on average (Fig. 12). The sites with the highest mean frequencies (F_{sarg}) were generally those with the highest frequencies of small influxes and not necessarily those with the most intense influxes. The sites also had different mean quantities of sargassum, i.e. mean P_{sarg} (Fig. 12). The sites displaying the highest quantities were not necessarily those with the greatest influx frequency.

Differences between sites are reflected in the daily dynamics of sargassum influx and pressure (Appendix A, Fig. A.5). The sites with the highest mean P_{sarg} were those where the quantity of sargassum varies the least over the year: Trésor (1), Cayol (3), Petit Galion (2), Pointe Hyacinthe (6) and Sable Blanc (7). At these sites, sargassum pressure was rarely zero, e.g. P_{sarg} never dropped below 25% at Trésor or below 10% at Cayol. In contrast, P_{sarg} fluctuations were much greater at Barrier of Cayol (4), Bourg du Robert (5), Barrier of Cap Est (8) and Anse Caffard (10). These sites can experience peaks of sargassum quantity during intense influxes, followed by a rapid decline of the sargassum pressure index.

Differences in exposure to sargassum influxes (F_{sarg}) and pressure (P_{sarg}) between sites can be explained by site's exposure angle and hydrodynamics (Fig. 13). The first two dimensions of the FAMD express 76% of the total inertia and are, therefore, sufficient for interpretation. The quantitative variables F_{sarg}, F_{medium} and *Exposure_angle* are significantly correlated with the first dimension (p-value < 0.05). The quantitative variable P_{sarg} and the qualitative variable *Hydrodynamics* are significantly correlated with the second dimension (p-value < 0.05). Thus, the exposure angle influences the influx frequency (F_{sarg}), while

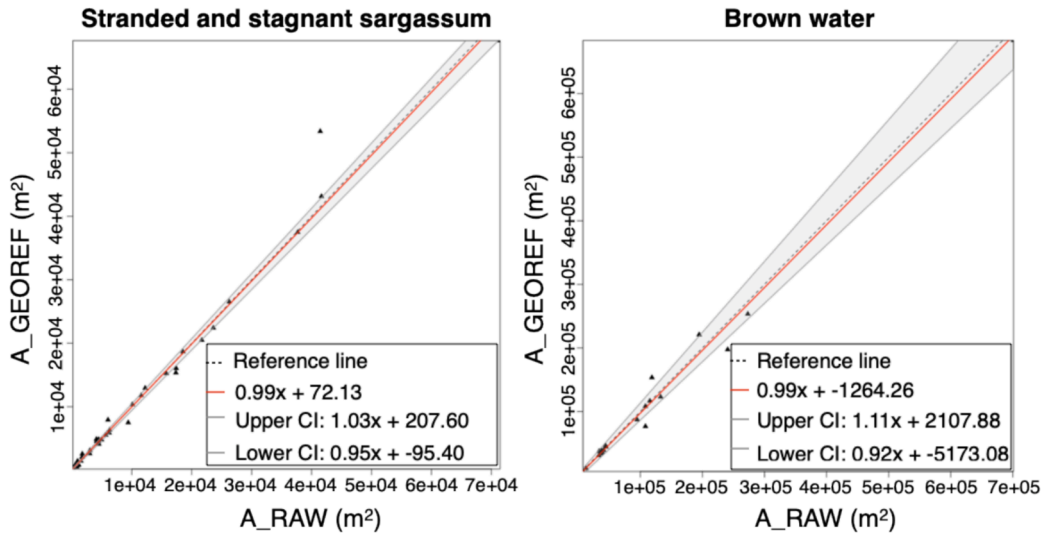

Fig. 9. Passing-Bablok regression comparing sargassum area measured by the "raw method" (A_RAW) to sargassum area measured by the "georef method" (A_GEOREF) for stranded/stagnant sargassum and brown water. Linear equations are represented as $y = b \times x + a$, with b the gradient and a the y-intercept. The red line represents the line of best-fit and the gray lines represent the upper and lower 95 % Confidence Interval (CI).

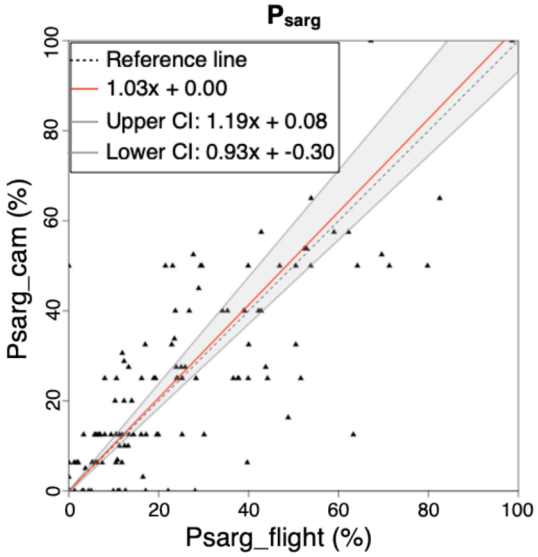

Fig. 10. Passing-Bablok regression to compare two methods (flight *vs.* camera) for calculating P_{sarg}. Linear equations are represented as $y = b \times x + a$, with b the gradient and a the y-intercept. The red line represents the line of best-fit and the gray lines represent the upper and lower 95 % Confidence Interval (CI).

hydrodynamics influence the level of sargassum pressure (P_{sarg}). The frequency of medium influxes is the highest, along with that of small influxes (Fig. 12), and is positively correlated with the exposure angle (Fig. 13). Consequently, F_{medium} is representative of the sites' overall exposure to influxes. On the other hand, large influxes (F_{large}) are strongly positively correlated with the sargassum pressure index, reflecting large accumulations of sargassum over time. The distribution of sites on the graph of individuals and categories (Fig. 13) is consistent with the results shown in Figs. 12 and A.5. Sites are plotted on the horizontal axis according to their exposure to influx: the lowest on the left with Taupinière (site 9), the highest on the right with Anse Caffard (site 10). They are then divided on the second bisector according to their level of sargassum pressure: the lowest, bottom left, with Taupinière, the highest, top right, with Trésor (site 1). To the exception of Cayol (site 3), the sites with the largest exposure angle are those with the highest frequency of medium influxes: Barrier of Cap Est (site 8), then Barrier of Cayol (site 4), and to a lesser extent Anse Caffard and Trésor. Barrier of Cap Est, Barrier of Cayol and Anse Caffard are the only sites with high hydrodynamics.

3.4. Seasonal dynamics of sargassum influxes and pressure at the scale of Martinique

Our local observations, i.e. the monthly influx frequency (F_{sarg}), the sargassum pressure index (P_{sarg}), and the area of stranded and stagnant sargassum and brown water show a similar pattern over time with the biomass of sargassum in the Central Atlantic Ocean and the influx risk of Météo France and NOAA/USF forecast bulletins (Fig. 14). This collinearity is statistically confirmed by the correlation matrix (Fig. 15). All these variables, except the brown water area, are significantly positively correlated (Spearman test, p-value < 0.05).

In 2022, the sargassum biomass in the Central Atlantic Ocean clearly increased from April onwards, peaked in June, and declined to very low levels from October to the end of the year (Fig. 14.A). In contrast, 2023 saw a marked increase in biomass from January onwards, peaking in March and gradually declining to reach its lowest value in November. Forecasts and observed sargassum influxes (F_{sarg}) and pressure (P_{sarg}) in Martinique were generally consistent with these trends, but we noted several differences. In 2022, the peak influx of sargassum (and peak pressure) in Martinique occurred in August, two months after the biomass peak observed in the Atlantic. The peak influx of sargassum in February 2023 did not coincide with an increase in sargassum biomass in the Atlantic Ocean. The intensity of sargassum influxes and pressure in February 2023 was similar to that observed in August 2022 (≈50% and 40%, respectively). The biomass peaked in March 2023 (13 million tons) but remained much lower than in June 2022 (20.4 million tons). In addition, the risk predicted by Météo France declined more drastically from April 2023 than the sargassum biomass, influx frequency and pressure.

Changes in the surface area of stranded (Fig. 14.B) and stagnant (Fig. 14.C) sargassum over time measured through aerial monitoring were generally consistent with F_{sarg} and P_{sarg} values calculated from *in situ* camera monitoring (Fig. 14.A). However, the dynamics differed among the three sargassum states (stranded, stagnant, and brown water). Area variability was much more pronounced for stagnant sargassum than for other states, with three peaks in August 2022 (187 ha), in January 2023 (213 ha) and in February 2023 (229 ha). During

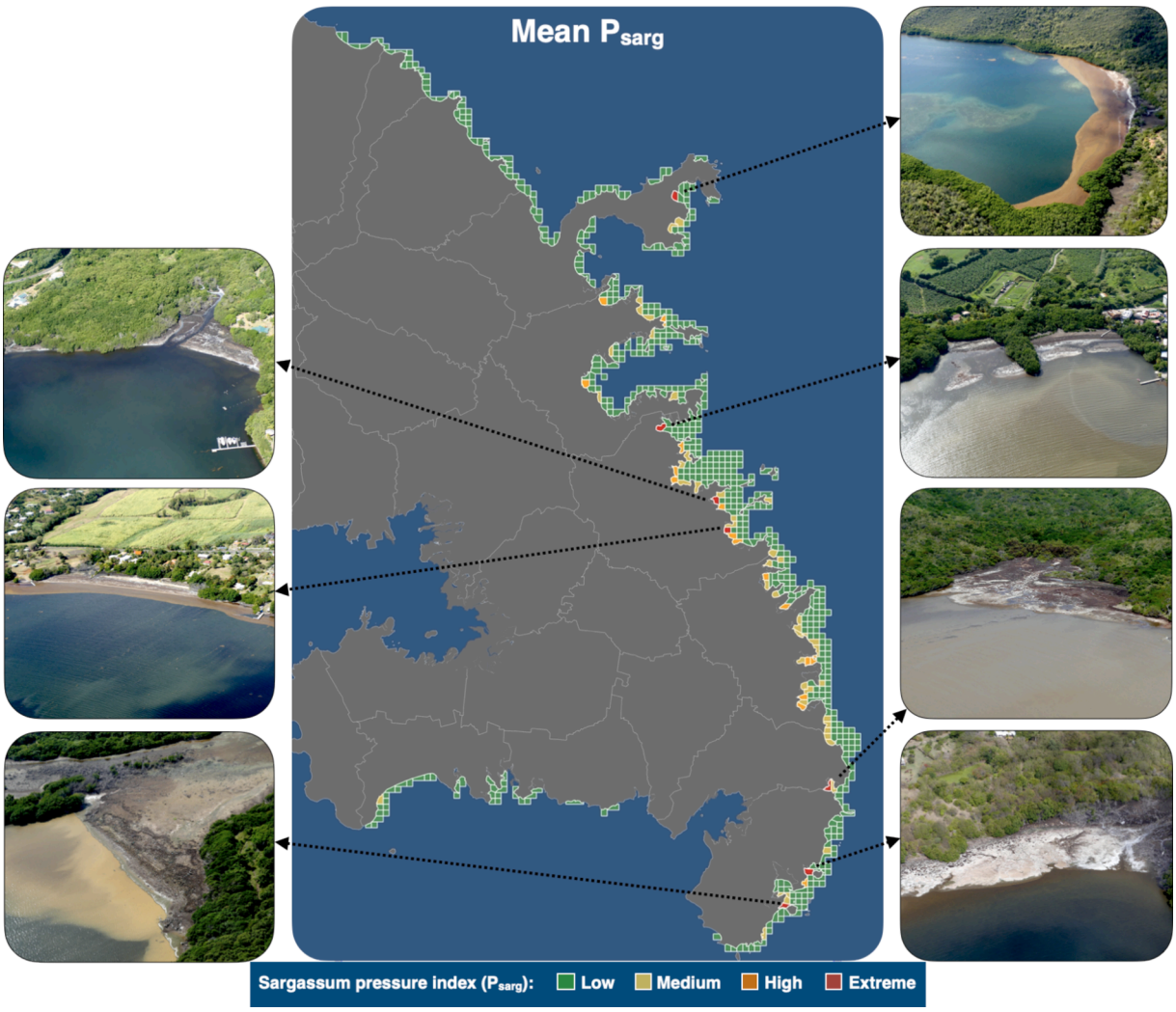

Fig. 11. Mean value of the sargassum pressure index (P_{sarg}) over the 20 flights in each cell along the coast of Martinique. Grid cells with an extreme average pressure (mean $P_{sarg} \geq 50$ %) are illustrated by aerial photography.

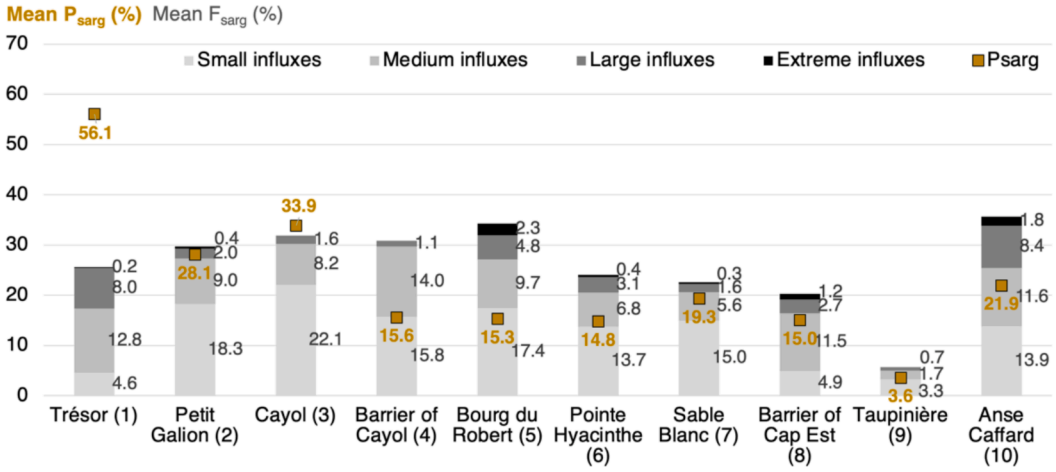

Fig. 12. Mean sargassum pressure index (Mean P_{sarg}) and mean frequency of influx according to influx intensity (Mean F_{sarg}) between January 2022 and December 2023 at each *in situ* camera-monitored site.

the lull in influxes (October to December), the surface area of stranded sargassum remained unchanged in 2022, whereas it was very low in 2023, with practically only low-density stranded sargassum. We observed the opposite for stagnant sargassum. In calm periods, the proportion of extreme density accumulations predominated in both 2022 and 2023. Changes in the surface area of brown water over time

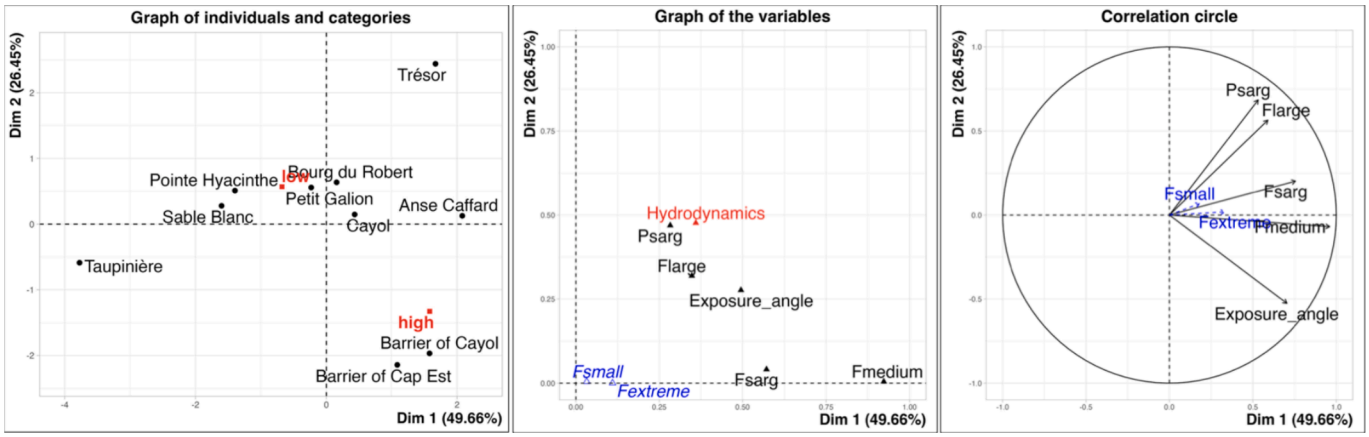

Fig. 13. Factor Analysis of Mixed Data (FAMD) graphs. Individuals: *in situ* camera-monitored sites. Categorical variables (red): Hydrodynamics (low/high). Quantitative variables: mean sargassum pressure index (P_{sarg}), mean frequency of influx (F_{sarg}), mean frequency of medium influx (F_{medium}), mean frequency of large influx (F_{large}), bay exposure angle (Exposure_angle). Supplementary quantitative variables (blue): mean frequency of small influx (F_{small}), mean frequency of extreme influx ($F_{extreme}$).

(Fig. 14.C) differed from that of stranded and stagnant sargassum. Brown water spread over a much larger area, peaking in September 2022 at 2,200 ha and July 2023 at 1,600 ha. Moreover, the surface area of brown water was only correlated to the area of stranded sargassum (Fig. 15). However, we noted that monthly variations in the surface area of brown water have closely followed variations in mean precipitation up to August 2023.

3.5. *Exposure of coastal marine communities to sargassum*

Assessing sargassum pressure along Martinique's coast revealed that marine communities are mainly exposed to brown water (Table 6). About 53% of the fringe mangrove occurring around the island is affected by sargassum, representing 46 km in total, 22 km of which are exposed to stagnant sargassum. Mangroves face a significantly higher proportion of high-density and extreme-density sargassum than other coastal communities. The largest exposed areas were recorded for seagrass communities, with 13% of the area occurring in Martinique (about 730 ha) affected by sargassum. Of this, 22 ha are subject to high-density sargassum, while 5 ha face extreme-density sargassum. About 7% of mixed communities, consisting of seagrass, algae, coral, sponge, and/or gorgonian species, are exposed to sargassum. In contrast, algal communities, sponge and gorgonian communities, and coral communities are the least affected, with only 1.2%, 0.5%, and 0.3% of their surface areas exposed, respectively.

4. Discussion

We have developed a methodology that combines two complementary monitoring approaches in space and time, allowing us to assess the pressure exerted by sargassum at the scale of Martinique. The validation tests (Figs. 9 and 10) and the consistency of our results with external data (Figs. 14 and 15) demonstrated the reliability of the new method. This work achieved the objective of quantifying sargassum pressure across Martinique using locally available tools, with the future goal of assessing the response of coastal ecosystems to varying levels of sargassum pressure. If this method is suitable for a territorial diagnosis, it is currently too complex and costly to be used for routine monitoring in Martinique or other territories. The main disadvantage of the aerial monitoring method is the time of the digitisation process, even without the additional step of georeferencing. In addition, it is recommended to fly vertically over the coastline to facilitate the processing of aerial images. However, with only 1.5 h of flight time to cover the exposed coastline, we were forced to cut across bays and move away from the coastline to save time, resulting in oblique photographs requiring a well-trained eye for adequate interpretation. Besides, brown water is more complicated to digitise rather than sargassum accumulations because there are fewer reference points in the open sea. Although brown water could also be confused with other sources of organic matter, such as estuarine discharges, it is important to note that León-Pérez et al. (2023) successfully distinguished their spectral signature using a multi-index approach, combining Sentinel-2 spectral bands with vegetation, seaweed, water, and water quality indices. Moreover, in this study, we demonstrate that it is generally possible to visually detect brown water, as it is often physically connected to its source – coastal sargassum accumulations, which were also digitised. Our data and observations showed that brown water was typically darker than estuarine discharges, which can be attributed to the large quantities of phlorotannins, polyphenols present only in *Phaeophyceae*, released by decaying sargassum (Powers et al., 2019). To ensure data quality, brown water was not digitised when the source of the coloration was uncertain, such as in areas where mixing occurs near estuaries. The peaks in stagnant sargassum observed in August 2022, January 2023, and February 2023 (Fig. 14) highlight another limitation of aerial monitoring: each flight represents a snapshot in time, which means the surface area measured can vary significantly depending on the time at which the survey occurred. Flights taken during massive sargassum influxes, of which the three peaks are a representation, revealed a considerably large area of sargassum. A few hours later, after the rafts accumulated on the coast, the area observed would have been much smaller (Appendix A, Fig. A.3). Hence, there is a need to consider sargassum density and supplement the data with daily monitoring to obtain dynamic information. However, the frequency of flights in our study was largely sufficient to characterise the average coastal exposure to sargassum pressure, while accounting for seasonal and interannual variability. Finally, aerial monitoring obviously depends on the availability of an aircraft, and the associated costs vary depending on the equipment used and the service provider. The cost and processing time are not suitable for daily monitoring, and additional *in situ* camera monitoring is needed to assess temporal patterns. However, a successful camera installation requires certain conditions that limit the sites that can be monitored. These conditions include a network connection, a suitable field of vision, a secure place to prevent theft, and sufficient light for the solar panel. Brown water is particularly difficult for the camera to detect because of the angle of view and the light conditions. In addition, the further away the camera is installed from the site, the more difficult it is to detect sargassum influxes, particularly small ones. This is probably why Trésor (site 1) and Barrier of Cap Est (site 8) have the lowest frequency of small influxes

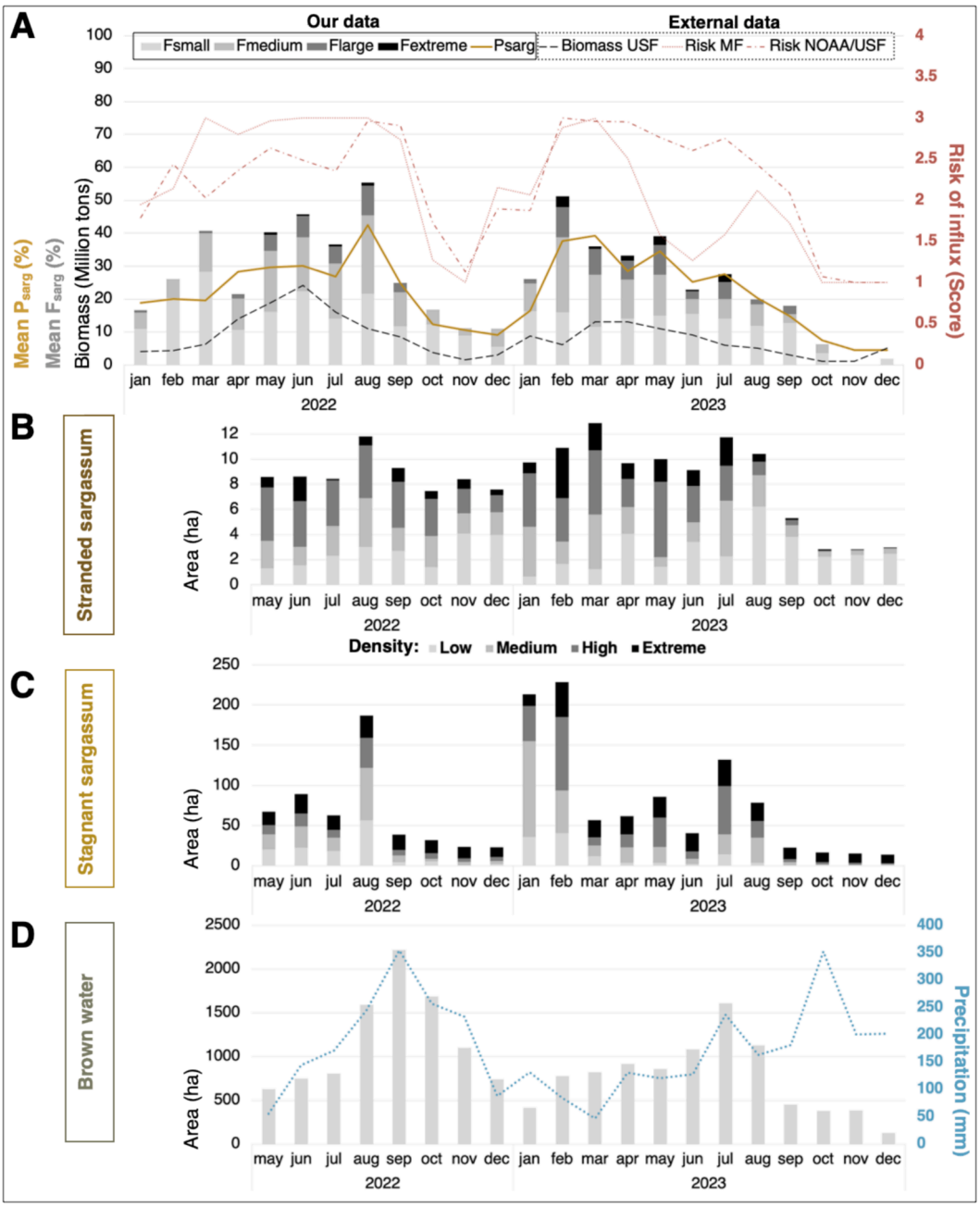

Fig. 14. Monthly dynamics of sargassum influxes and associated pressure in Martinique from January 2022 to December 2023 (A). Monthly variations in the area of stranded sargassum (B), stagnant sargassum (C) and brown water (D) in Martinique from May 2022 to December 2023. Our data: F_{small}, F_{medium}, F_{large}, $F_{extreme}$ represent the mean influx frequency (F_{sarg}) according to the influx intensity among all *in situ* camera-monitored sites. P_{sarg} represents the mean sargassum pressure index (total quantity / theoretical maximum quantity x 100) among all *in situ* camera-monitored sites. Areas of stranded/stagnant sargassum and brown water were calculated by summing the area of all sargassum features of each flight. External data: see Table 4.

while they have the highest frequency of medium influxes (Fig. 12). There may, therefore, be an underestimation of influxes depending on the site. Given these limitations, other tools may be considered for quantifying sargassum pressure. For instance, Degia et al. (2024) used Google Earth Pro to create sargassum inundation hazard maps for Barbados, a small Caribbean island. They employed a simple, cost-effective approach to identify areas, mainly beaches, exposed to sargassum and coastal assets, generating valuable planning tools for the entire island. However, sargassum quantification is less precise, relying on a three-class magnitude index without actual area measurements. Additionally, brown water is not considered, and no distinction is made between stranded and stagnant sargassum. This approach could be suitable for territories with limited data acquisition resources, offering an overview of priority sites. However, it does not quantify the spatial extent of sargassum pressure on the coastal environment. It is also less suitable for territories like Martinique, where most of the exposed coastline consists of mangrove habitats or urbanised areas. Sargassum typically cannot strand on these types of coasts and remains stagnant. Therefore, it is particularly important to measure both the surface area and the density, which can vary greatly, in order to accurately estimate sargassum pressure. Although improvements are required to adapt it for routine monitoring, our method provides key information on the spatial variability and dynamics of sargassum pressure, distinguishing between stranded sargassum, stagnant sargassum, and brown water. The

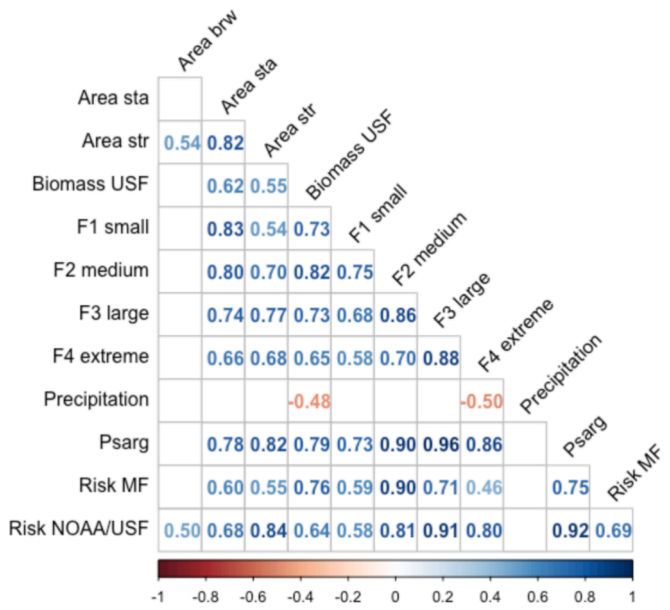

Fig. 15. Correlation matrix between our local observations of sargassum and external data (monthly means, all sites combined). Our data: influx frequency according to the intensity of influx event (F1 small, F2 medium, F3 large, F4 extreme), sargassum pressure index (P_{sarg}), area of stranded sargassum (Area str), stagnant sargassum (Area sta) and brown water (Area brw). External data: see Table 4. Only significant correlation coefficients are displayed (Spearman test, p-value < 0.05).

differentiation of these three decomposition states will enable the subsequent assessment of their respective impacts on the ecosystems they threaten.

Aerial monitoring identified the most exposed sites to sargassum pressure during the 20 flights (Figs. 11 and A.4) and confirmed our hypothesis. They are all located inside bays with low hydrodynamics; most are mangroves. Most are exposed to prevailing winds, which are the northeast trade winds. The exposure angle determines the exposure to sargassum influxes, which influences the intensity of sargassum accumulations, while hydrodynamic conditions control the residence time of these accumulations. This is well illustrated by our detailed analysis of influx dynamics and pressure levels at contrasting sites, which were monitored daily by cameras (Figs. 12, 13, A.5). The sites with the most frequent influxes (F_{sarg}) are those with the widest angle of exposure, facilitating the entry of sargassum rafts in the bay (Fig. 2). However, these sites can have very different sargassum accumulation dynamics, depending on their hydrodynamics (Fig. A.5). Sites with low hydrodynamics showed sargassum accumulations throughout the study period, suggesting that the consequence of low hydrodynamics is prolonged exposure to sargassum pressure. As sedimentation zones, the innermost parts of the bays are particularly affected. This is particularly true in mangroves (Fig. 11), where sargassum remains trapped for longer periods. The extremely low decomposition rate of soil organic matter in mangrove forests (Middleton and McKee, 2001) could explain the persistence of decaying sargassum all over the year, even during lulls in massive influxes. Hence, the duration of exposure to sargassum largely depends on the rate of its degradation in areas with low hydrodynamic conditions. The dynamics of sargassum accumulation can significantly vary at sites with high hydrodynamics (Fig. A.5). A large quantity of sargassum can momentarily invade a site and quickly disappear over the following days. We observed that energetic waves can effectively remove stranded and stagnant sargassum accumulated nearshore and transfer them offshore, as previously observed by Rutten et al. (2021). At sites 4 and 8, equipped with sargassum barriers, we observed that sargassum rafts pass through the reef channels and accumulate along the sargassum barrier, remaining close to the reef channels. Strong currents in the channels can remobilise stagnant sargassum and export them outside the barrier reef. Consequently, in coastal areas with strong hydrodynamics, the exposure time to sargassum depends mainly on swell and current conditions, which are influenced by meteorological conditions. The methods employed to collect sargassum can also influence the level of pressure. Offshore collection operations (e.g. at sites 4, 5, and 8) reduce the residence time of accumulations. At Bourg du Robert (site 5), a sargassum barrier facilitates the convergence of sargassum rafts towards a designated collection point on land equipped with a backhoe loader. This may explain why an inner part of the bay, like site 5, has a relatively average pressure level despite having one of the highest influx frequencies (Fig. 12). However, it was observed that sargassum barriers are degrading rapidly due to their year-round immersion and the forces generated by currents and sargassum accumulations. It can happen, therefore, that they break, and all or part of stagnant sargassum previously retained by the barrier reaches the coast. This could explain the high level of sargassum pressure at Cayol (site 3), which is usually protected by the sargassum barrier.

While the exposure angle and hydrodynamics drive spatial variations, the dynamics of sargassum growth and transport in the Atlantic Ocean influence temporal variations in the frequency and intensity of influxes (Figs. 14 and 15). In 2022, the Atlantic sargassum biomass peaked in June, and massive influxes occurred on the coast of Martinique in August. This 2-month time lag coincides with the results of Putman et al. (2018) on the sargassum transport pathways from the Equatorial Atlantic to the Caribbean Sea. The authors found that sargassum rafts drifting with the North Brazil Current and the Guiana Current in spring generally reach the Caribbean in two months. The seasonal patterns observed in 2022 were consistent with those documented in previous years, with biomass peaks occurring in June (2018, 2020, 2021) or July (2015, 2019) (University of South Florida, 2024). In contrast, 2023 showed a particular seasonality, with an early increase in sargassum biomass from January to April, without the usual bloom in June. Since June 2023, record-breaking temperatures have been recorded across the globe as a consequence of climate change (World Meteorological Organization (WMO), 2024). According to the work of Hanisak and Samuel (1987), the maximum sargassum growth occurs at temperatures ranging from 22 to 28 °C. Exceptional sea surface

Table 6
Maximum area (ha) or coastal length (km) of coastal marine communities exposed to sargassum in Martinique as recorded during the 20 flights, compared to the total area or coastal length of these communities at the scale of Martinique (%). The columns 'All densities' and 'All states' both represent the maximum area or coastal length of sargassum recorded from a single flight out of the 20, with 'All densities' disregarding density and 'All states' disregarding decomposition state. Mixed communities = seagrass, algae, coral, sponge and/or gorgonian species.

Coastal marine communities	Brown water	Stagnant sargassum					All states	% Total Martinique
		Low density	Medium density	High density	Extreme density	All densities		
Algae (ha)	91	15	9	2	0	24	107	1.2
Coral (ha)	13	1	1	0	0	2	13	0.3
Mixed (ha)	16	1	1	1	0	2	16	6.7
Sponge and Gorgonian (ha)	3	8	1	0	0	8	8	0.5
Seagrass (ha)	724	6	35	22	5	53	731	13.0
Mangrove (km)	24	4	12	9	7	22	46	52.9

temperature recorded in 2023 may have influenced sargassum population dynamics and prevented the summer bloom. Moreover, the 2023 El Niño–Southern Oscillation (ENSO), associated with higher air temperatures, resulted in precipitation deficits over Mexico and the Amazon (WMO, 2024). This event may also have limited population growth by reducing the Amazon's discharges, which are known to be a nutrient source for sargassum (Lapointe et al., 2021). It should also be noted that the intensity of sargassum influxes in Martinique does not appear to be proportional to the sargassum biomass in the Atlantic Ocean. In June 2022, sargassum biomass reached a record of 24.2 million tonnes, surpassing the previous record of 20.4 million tonnes in June 2018 (Wang et al., 2019). In January 2023, the biomass of sargassum was 8.7 million tonnes. Although this figure represents a record for this month compared with previous years, it remains well below the values recorded in June 2022 (University of South Florida, 2024). However, the peak influxes observed in Martinique in August 2022 was relatively similar to that of February 2023 (Fig. 14.C). This is also the case for the sargassum pressure index. This result highlights the limitations of satellite observations in forecasting the location and intensity of nearshore influxes at the local scale, given the local hydrodynamics, winds and coastal configurations. However, they can be good indicators of sargassum pressure on a territorial scale.

Furthermore, it seems crucial to differentiate the various states of sargassum (stranded, stagnant and brown water) when characterising the coastal pressure, as they have distinct dynamics (Fig. 14.B, C, D). During the lull in sargassum influxes, from October to December, most of the stranded sargassum has a low density (Fig. 14.B), whereas stagnant sargassum has almost exclusively an extreme density (Fig. 14.C). This contrast in density is probably due to the difference in the decomposition rate of sargassum in the open air and in water. Studies have shown that 48 h of sun exposure is enough to dry out stranded sargassum, resulting in a rapid decline in its density (Tonon et al., 2022; Trench et al., 2022; Paredes-Camacho et al., 2023). For stagnant sargassum, the decomposition rate of organic matter in water can be extremely low, particularly in mangroves (Mcleod et al., 2011). In these areas, the density remains very high all year round, as observed at Trésor (Appendix A, Fig. A.5). Regarding brown water dynamics, we noted a correlation between changes in brown water surface area and the seasonality of precipitations (Fig. 14.D). Estuaries and mangroves are the areas where brown water diffusion is the greatest (Appendix A, Fig. A.4). Heavy precipitation induces an increase in river discharge and an extension of the turbid plume at the mouth of estuaries (Lahet and Stramski, 2010). If there are massive accumulations of sargassum around the estuary mouth, brown water can extend offshore as the flow increases. Tidal currents can also reinforce this phenomenon. In mangroves, heavy rainfall can play an important role in sediment resuspension and offshore export because currents induced by rainwater runoff during ebb tides can be more intense than tide-induced currents (Schwarzer et al., 2016). Consequently, the remobilisation of high-concentrated sargassum debris trapped in mangroves can also occur, leading to the offshore dispersion of brown water through rainwater runoff.

Finally, quantifying and locating sargassum pressure at Martinique's scale highlighted the territory's current environmental challenges. Our results revealed that mangroves and seagrass meadows are the most exposed marine coastal habitats to sargassum pressure (Table 6). Over one-fifth of the total seagrass area and half of the total fringe mangrove line are exposed to sargassum pressure. Mangroves appear to be the main receptacle for extremely dense and persistent accumulations of sargassum along coastal areas. The consequences of this new source of eutrophication can lead to mangrove death (Lovelock et al., 2009; Hernandez et al., 2020). Further from the coast, seagrass meadows and mixed communities are mainly exposed to brown water. van Tussenbroek et al. (2017) observed that sargassum brown tide caused the mortality of coral colonies and the replacement of the seagrass climax species *Thalassia testudinum* by macroalgae. Our findings are, therefore, highly alarming, as mangroves, seagrass meadows and coral reefs are vulnerable ecosystems already subject to numerous anthropogenic pressures (Goldberg and Wilkinson, 2004; Grech et al., 2012; Turschwell et al., 2020). Future research is required to assess the state of coastal ecosystems in relation to sargassum pressure levels, which will be the focus of our upcoming work.

5. Conclusion

The methodology developed in this study allows for a better characterisation of spatial and temporal variations in coastal sargassum pressure at the island scale. This case study has improved our general knowledge of the pressure dynamics, depending on the state of decomposition of sargassum (stranded, stagnant, brown water), the location of influxes and the time of year. Our substantial sampling effort provides valuable data for managers, researchers and entrepreneurs in Martinique and other territories in the Caribbean and beyond that face health, socio-economic, and environmental issues due to sargassum brown tides. This is of great interest to local authorities, as it enables the identification of sites at stake (via aerial monitoring) and periods at risk (via *in situ* camera monitoring). This includes locating the areas most susceptible to sargassum accumulation and the spatial extent of brown water towards the open sea. This latter information is particularly valuable for assessing the exposure of marine habitats to sargassum pressure. Daily observations of sargassum influxes and accumulations are also helpful for stakeholders and residents to adapt their responses according to pressure level. Indeed, the local variability of sargassum influxes justifies the implementation of *in situ* monitoring alongside forecast bulletins, allowing for more efficient and cost-effective management through pressure-adjusted interventions. Near-real-time monitoring also provides important insights for future sargassum valorisation companies. Local observations are complementary to satellite data used in current forecasting and can also be used to improve stranding forecast algorithms. Depending on the objectives, it is possible to use aerial or *in situ* camera-only monitoring. However, we recommend combining the two methods for a complete assessment of sargassum pressure in the study area (spatial extent and dynamics). Territorial diagnosis could be followed by long-term *in situ* camera monitoring in high-risk areas, where management actions are a priority. In this case, our method could be improved by AI algorithms, which have been used in several studies (Valentini and Balouin, 2020; Rutten et al., 2021; Arellano-Verdejo et al., 2022; Uribe-Martinez et al., 2022). Combining our density score with automatically detected areas would reduce the time required for data acquisition and processing. It would also be helpful to conduct field measurements of sargassum volume under various conditions, for example, for each density class defined in this study. This would improve the accuracy of sargassum quantification, which is particularly important for adjusting collection operations. Periodic flights could be maintained for long-term monitoring to verify the effectiveness of management measures, particularly the reduction in the spatial extent of sargassum pressure. The choice of methodology and precision for quantifying sargassum pressure depends on available resources and objectives and must be adapted to the specific features of each territory.

Funding

This work was supported by the Martinique Marine Natural Park and the French Biodiversity Agency (OFB) through the French Government's France Relance program (n° OFB-21–0875, 2021–2023), the Martinique Water Office (ODE) (n° 001–01-2022, 2022–2024), the Martinique Department of the Environment, Land Planning and Housing (DEAL) (n° 001–05-2022, 2022–2024), and the National Association for Research and Technology (ANRT) through a CIFRE grant (n° 2021/1624, 2022–2025).

CRediT authorship contribution statement

Mathilde Teyssier: Writing – review & editing, Writing – original draft, Methodology, Investigation, Funding acquisition, Formal analysis, Data curation, Conceptualization. **Catherine Desrosiers:** Writing – review & editing, Project administration, Funding acquisition. **Claire Hellio:** Writing – review & editing, Supervision, Funding acquisition. **Fanny Kerninon:** Writing – review & editing, Supervision, Funding acquisition.

Declaration of competing interest

The authors declare that they have no known competing financial interests or personal relationships that could have appeared to influence the work reported in this paper.

Acknowledgments

We thank Fabien Védie (DEAL Martinique) for his help in conceptualising the method, Olivier Perronnet (PNMM), Paul Giannasi (PNMM) and Mélissa Bocaly (ODE) for their contribution in selecting sites, Sophie de Naurois-Turgot (Aerodream) for piloting the gyrocopter, Dr Mélanie Bon, Dr Florian de Bettignies, Dr Jonathan Migeot, Antoine Tobie and Guillaume Tollu (Impact Mer) for their participation in the aerial monitoring, Clément Bouvier (BRGM Martinique) for providing access to historical camera data, Olivia Amintas and Carole Boulanger (Madininair) for camera installation and maintenance, residents for hosting cameras, Prof Olivier Gros (Université des Antilles), Prof Iwan Le Berre (Université de Bretagne Occidentale) and Dr Lydiane Mattio (bluecweed) for reviewing the manuscript. Finally, we would like to thank the three anonymous reviewers for their valuable contributions.

Appendix A. Supplementary data

Supplementary data to this article can be found online at https://doi.org/10.1016/j.ecolind.2025.113211.

Data availability

Data will be made available on request.

References

Actimar, 2020. Projet Carib-Coast, Tâche 3 - Premières modélisations. Rapport final pour le compte de Ifremer. RED-1693.

Arellano-Verdejo, J., Lazcano-Hernández, H.E., 2021. Collective view: mapping *Sargassum* distribution along beaches. PeerJ Comput. Sci. 7, e528.

Arellano-Verdejo, J., Santos-Romero, M., Lazcano-Hernandez, H.E., 2022. Use of semantic segmentation for mapping Sargassum on beaches. PeerJ 10, e13537. https://doi.org/10.7717/peerj.13537.

Baldwin, K., Oxenford, H.A., Weekes, J., Small, M., Irvine, J., Desai, A., 2022. Sargassum Monitoring Protocol: monitoring sargassum abundance using drones. SargAdapt Good Practice Guide Series 1. University of the West Indies, Centre for Resource Management and Environmental Studies (UWI CERMES), Barbados, p. 40.

Barbier, E.B., Hacker, S.D., Kennedy, C., Koch, E.W., Stier, A.C., Silliman, B.R., 2011. The value of estuarine and coastal ecosystem services. Ecol. Monogr. 81, 169–193. https://doi.org/10.1890/10-1510.1.

Bouvier, C., 2024. Suivi des échouages de sargasses sur le littoral de la Martinique (2022-2023). Rapport final V1. BRGM/RP-73581-FR, 8 p.

Centre for Resource Management and Environmental Studies, 2024. Sub-regional Sargassum Outlook Bulletin. https://www.cavehill.uwi.edu/cermes/research-projects/sargassum/outlook-bulletin.aspx.

Collado-Vides, L., van Tussenbroek, B., Garcia, M., Rodríguez-Martínez, R., Cassano, V., Oliveira, M., ... & Krueger-Hadfield, S., 2018. A network to develop a taxonomic, monitoring, and citizen's participation program for Sargassum landings in Florida, Mexico, Barbados, and Brazil. Proceedings of the Gulf and Caribbean Fisheries Institute (Vol. 71, pp. 319-324).

Degia, A.K., Small, M., Oxenford, H.A., 2024. Applying the Disaster Risk Assessment Framework to *Sargassum* Inundation in Barbados. Gulf and Caribbean Research 35 (1), GCFI14-GCFI29. https://doi.org/10.18785/gcr.3501.11.

Fidai, Y.A., Dash, J., Tompkins, E.L., Tonon, T., 2020. A systematic review of floating and beach landing records of Sargassum beyond the Sargasso Sea. Environ. Res. Commun. 2, 122001. https://doi.org/10.1088/2515-7620/abd109.

Franks, J.S., Johnson, D.R., Ko, D.S., 2016. Pelagic Sargassum in the Tropical North Atlantic. Gulf Caribb. Res. 27. https://doi.org/10.18785/gcr.2701.08.

Goldberg, J., Wilkinson, C., 2004. Global threats to coral reefs: coral bleaching, global climate change, disease, predator plagues and invasive species. Status of Coral Reefs of the World 2004, 67–92.

Gower, J., Young, E., King, S., 2013. Satellite images suggest a new *Sargassum* source region in 2011. Remote Sens. Lett. 4, 764–773. https://doi.org/10.1080/2150704X.2013.796433.

Grech, A., Chartrand-Miller, K., Erftemeijer, P., Fonseca, M., McKenzie, L., Rasheed, M., Taylor, H., Coles, R., 2012. A comparison of threats, vulnerabilities and management approaches in global seagrass bioregions. Environ. Res. Lett. 7, 024006. https://doi.org/10.1088/1748-9326/7/2/024006.

Hanisak, M.D., Samuel, M.A., 1987. Growth rates in culture of several species of Sargassum from Florida, USA. In: Ragan, M.A., Bird, C.J. (Eds.), Twelfth International Seaweed Symposium. Springer, Netherlands, Dordrecht, pp. 399–404.

Hernandez, W.J., Morell, J.M., Armstrong, R.A., 2020. High-Resolution Satellite Imagery to Assess *Sargassum* Inundation Impacts to Coastal Areas. bioRxiv 2020.08.10.244004. https://doi.org/10.1101/2020.08.10.244004.

Hu, C., Wang, M., Lapointe, B.E., Brewton, R.A., Hernandez, F.J., 2021. On the Atlantic pelagic Sargassum's role in carbon fixation and sequestration. Sci. Total Environ. 781, 146801. https://doi.org/10.1016/j.scitotenv.2021.146801.

Iporac, L.A.R., Hatt, C., D., K., Bally, N., Castro, A., 2022. Community-based monitoring reveals spatiotemporal variation of sargasso inundation levels and morphotype dominance across the Caribbean and South Florida. Aquat. Bot. 182, 103546.

Johns, E.M., Lumpkin, R., Putman, N.F., Smith, R.H., Muller-Karger, F.E., Rueda-Roa, T., D.,, Hu, C., Wang, M., Brooks, M.T., Gramer, L.J., Werner, F.E., 2020. The establishment of a pelagic Sargassum population in the tropical Atlantic: Biological consequences of a basin-scale long distance dispersal event. Prog. Oceanogr. 182, 102269. https://doi.org/10.1016/j.pocean.2020.102269.

Lahet, F., Stramski, D., 2010. MODIS imagery of turbid plumes in San Diego coastal waters during rainstorm events. Remote Sens. Environ. 114, 332–344. https://doi.org/10.1016/j.rse.2009.09.017.

Lapointe, B.E., Brewton, R.A., Herren, L.W., Wang, M., Hu, C., McGillicuddy, D.J., Lindell, S., Hernandez, F.J., Morton, P.L., 2021. Nutrient content and stoichiometry of pelagic Sargassum reflects increasing nitrogen availability in the Atlantic Basin. Nat. Commun. 12, 3060. https://doi.org/10.1038/s41467-021-23135-7.

Le, S., Josse, J., Husson, F., 2008. FactoMineR: An R package for multivariate analysis. J. Stat. Software 25 (1), 1–18. https://doi.org/10.18637/jss.v025.i01.

León-Pérez, M.C., Reisinger, A.S., Gibeaut, J.C., 2023. Spatial-temporal dynamics of decaying stages of pelagic Sargassum spp. along shorelines in Puerto Rico using Google Earth Engine. Mar. Pollut. Bull. 188, 114715. https://doi.org/10.1016/j.marpolbul.2023.114715.

Lovelock, C.E., Ball, M.C., Martin, K.C., Feller, C., I., 2009. Nutrient enrichment increases mortality of mangroves. PLOS ONE 4, e5600.

Maréchal, J.-P., Hellio, C., Hu, C., 2017. A simple, fast, and reliable method to predict Sargassum washing ashore in the Lesser Antilles. Remote Sens. Appl. Soc. Environ. 5, 54–63. https://doi.org/10.1016/j.rsase.2017.01.001.

Marsh, R., Skliris, N., Tompkins, E.L., Dash, J., Dominguez Almela, V., Tonon, T., Oxenford, H.A., Webber, M., 2023. Climate-sargassum interactions across scales in the tropical Atlantic. PLOS Clim. 2, e0000253. https://doi.org/10.1371/journal.pclm.0000253.

Mcleod, E., Chmura, G.L., Bouillon, S., Salm, R., Björk, M., Duarte, C.M., Lovelock, C.E., Schlesinger, W.H., Silliman, B.R., 2011. A blueprint for blue carbon: toward an improved understanding of the role of vegetated coastal habitats in sequestering CO2. Front. Ecol. Environ. 9, 552–560. https://doi.org/10.1890/110004.

Mendez-Tejeda, R., Rosado, J., Gladys, A., 2019. Influence of climatic factors on Sargassum arrivals to the coasts of the Dominican Republic. J. Oceanogr. Mar. Sci. 10, 22–32. https://doi.org/10.5897/JOMS2019.0156.

Météo France, 2024. Bulletin de prévision d'échouement des sargasses pélagiques. https://meteofrance.mq/fr/sargasses.

Middleton, B.A., McKee, K.L., 2001. Degradation of Mangrove Tissues and Implications for Peat Formation in Belizean Island Forests. J. Ecol. 89, 818–828.

National Oceanic and Atmospheric Administration, University of South Florida, 2024. Experimental Weekly Sargassum Inundation Risk (SIR v1.3). https://cwcgom.aoml.noaa.gov/SIR/.

Nicet, J.B., 2024. Guide pour l'utilisation de la carte des habitats marins côtiers (0-40 m) de la Martinique. Rapport MAREX/AQUASEARCH pour le compte du Parc. Naturel Marin de Martinique (OFB) 27.

Ody, A., Thibaut, T., Berline, L., Changeux, T., André, J.-M., Chevalier, C., Blanfuné, A., Blanchot, J., Ruitton, S., Stiger-Pouvreau, V., Connan, S., Grelet, J., Aurelle, D., Guéné, M., Bataille, H., Bachelier, C., Guillemain, D., Schmidt, N., Fauvelle, V., Guasco, S., Ménard, F., 2019. From In Situ to satellite observations of pelagic Sargassum distribution and aggregation in the Tropical North Atlantic Ocean. PLOS ONE 14, e0222584. https://doi.org/10.1371/journal.pone.0222584.

Oviatt, C.A., Huizenga, K., Rogers, C.S., Miller, W.J., 2019. What nutrient sources support anomalous growth and the recent sargassum mass stranding on Caribbean beaches? A review. Mar. Pollut. Bull. 145, 517–525. https://doi.org/10.1016/j.marpolbul.2019.06.049.

Paredes-Camacho, R.M., González-Morales, S., González-Fuentes, J.A., Rodríguez-Jasso, R.M., Benavides-Mendoza, A., Charles-Rodríguez, A.V., Robledo-Olivo, A., 2023. Characterization of Sargassum spp. from the Mexican Caribbean and Its Valorization through Fermentation Process. Processes 11. https://doi.org/10.3390/pr11030685.

Passing, H., Bablok, 1983. A new biometrical procedure for testing the equality of measurements from two different analytical methods. Application of linear regression procedures for method comparison studies in clinical chemistry, Part I.

J. Clin. Chem. Clin. Biochem. 11, 709–720. https://doi.org/10.1515/cclm.1983.21.11.709.
Potapov, S., Model, F., Schuetzenmeister, A., Manuilova, E., Dufey, F., Raymaekers, J., 2023. mcr: Method Comparison Regression. R Package Version 1 (3), 3. https://CRAN.R-project.org/package=mcr.
Powers, L.C., Hertkorn, N., McDonald, N., Schmitt-Kopplin, P., Del Vecchio, R., Blough, N.V., Gonsior, M., 2019. Sargassum sp. act as a large regional source of marine dissolved organic carbon and polyphenols. Global Biogeochemical Cycles 33, 1423–1439. https://doi.org/10.1029/2019GB006225.
Pujos, M., Gonzalez, J.L., Pons, J.C., 1992. Circulation des eaux sur les plateaux insulaires de Martinique et Guadeloupe. Prost Marie-Thérèse (ed.). Evolution des littoraux de Guyane et de la zone caraïbe méridionale pendant le quaternaire. Paris : ORSTOM, p. 415-435. (Colloques et Séminaires). Symposium PICG 274/ORSTOM, Cayenne (GUF), 1990/11/09-14. ISBN 2-7099-1109-4.
Putman, N.F., Goni, G.J., Gramer, L.J., Hu, C., Johns, E.M., Trinanes, J., Wang, M., 2018. Simulating transport pathways of pelagic Sargassum from the Equatorial Atlantic into the Caribbean Sea. Prog. Oceanogr. 165, 205–214. https://doi.org/10.1016/j.pocean.2018.06.009.
QGIS.org, 2024. QGIS Geographic Information System. QGIS Association. http://www.qgis.org.
R Core Team, 2024. R: A language and environment for statistical computing. R Foundation for Statistical Computing, Vienna, Austria. https://www.R-project.org/.
Resiere, D., Valentino, R., Nevière, R., Banydeen, R., Gueye, P., Florentin, J., Cabié, A., Lebrun, T., Mégarbane, B., Guerrier, G., Mehdaoui, H., 2018. Sargassum seaweed on Caribbean islands: an international public health concern. The Lancet 392, 2691. https://doi.org/10.1016/S0140-6736(18)32777-6.
Rodríguez-Martínez, R.E., Medina-Valmaseda, A.E., Blanchon, P., Monroy-Velázquez, L. V., Almazán-Becerril, A., Delgado-Pech, B., Vásquez-Yeomans, L., Francisco, V., García-Rivas, M.C., 2019. Faunal mortality associated with massive beaching and decomposition of pelagic Sargassum. Mar. Pollut. Bull. 146, 201–205. https://doi.org/10.1016/j.marpolbul.2019.06.015.
Rodríguez-Martínez, R.E., Jordán-Dahlgren, E., Hu, C., 2022. Spatio-temporal variability of pelagic Sargassum landings on the northern Mexican Caribbean. Remote Sens. Appl. Soc. Environ. 27, 100767. https://doi.org/10.1016/j.rsase.2022.100767.
Rutten, J., Arriaga, J., Montoya, L.D., Mariño-Tapia, I.J., Escalante-Mancera, E., Mendoza, E.T., Tussenbroek, B.I., Appendini, C.M., 2021. Beaching and natural removal dynamics of pelagic sargassum in a fringing-reef lagoon. J. Geophys. Res. Oceans 126. https://doi.org/10.1029/2021JC017636.
Schwarzer, K., Thanh, N.C., Ricklefs, K., 2016. Sediment re-deposition in the mangrove environment of Can Gio, Saigon River estuary (Vietnam). J. Coast. Res. 138–142. https://doi.org/10.2112/SI75-028.1.
Skliris, N., Marsh, R., Appeaning Addo, K., Oxenford, H., 2022. Physical drivers of pelagic sargassum bloom interannual variability in the Central West Atlantic over 2010–2020. Ocean Dyn. 72, 383–404. https://doi.org/10.1007/s10236-022-01511-1.
Solarin, B.B., Bolaji, D.A., Fakayode, O.S., Akinnigbagbe, R.O., 2014. Impacts of an invasive seaweed Sargassum hystrix var. fluitans (Børgesen 1914) on the fisheries and other economic implications for the Nigerian coastal waters. IOSR J. Agric. Vet. Sci. 7, 01–06. https://doi.org/10.9790/2380-07710106.
Tonon, T., Machado, C.B., Webber, M., Webber, D., Smith, J., Pilsbury, A., Cicéron, F., Herrera-Rodriguez, L., Jimenez, E.M., Suarez, J.V., Ahearn, M., Gonzalez, F., Allen, M.J., 2022. Biochemical and elemental composition of pelagic sargassum biomass harvested across the caribbean. Phycology 2, 204–215. https://doi.org/10.3390/phycology2010011.
Trench, C., Thomas, S.-L., Thorney, D., Maddix, G.-M., Francis, P., Small, H., Machado, C. B., Webber, D., Tonon, T., Webber, M., 2022. Application of stranded pelagic sargassum biomass as compost for seedling production in the context of mangrove restoration. Front. Environ. Sci. 10, 932293. https://doi.org/10.3389/fenvs.2022.932293.
Turschwell, M.P., Tulloch, V.J.D., Sievers, M., Pearson, R.M., Andradi-Brown, D.A., Ahmadia, G.N., Connolly, R.M., Bryan-Brown, D., Lopez-Marcano, S., Adame, M.F., Brown, C.J., 2020. Multi-scale estimation of the effects of pressures and drivers on mangrove forest loss globally. Biol. Conserv. 247, 108637. https://doi.org/10.1016/j.biocon.2020.108637.
UNEP-CEP, 2021. Sargassum White Paper: Turning the crisis into an opportunity. United Nations Environment Programme and Caribbean Environment Programme.
University of South Florida, 2024. Satellite-based Sargassum Watch System (SaWS). Sargassum Outlook Bulletins. https://optics.marine.usf.edu/projects/saws.html.
Uribe-Martinez, A., Cha, V., Fontes, J.V.H., van Tussenbroek, B.I., Mariño-Tapia, I., Ojeda, E., Castañeda-Ram, D.G., Silva, R., 2022. Multiscale distribution patterns of pelagic rafts of sargasso (Sargassum spp.) in the Mexican Caribbean (2014–2020). Front. Mar. Sci. https://doi.org/10.3389/fmars.2022.920339.
Valentini, N., Balouin, Y., 2020. Assessment of a Smartphone-Based Camera System for Coastal Image Segmentation and Sargassum monitoring. J. Mar. Sci. Eng. 8, 23. https://doi.org/10.3390/jmse8010023.
van Tussenbroek, B.I., Hernández Arana, H.A., Rodríguez-Martínez, R.E., Espinoza-Avalos, J., Canizales-Flores, H.M., González-Godoy, C.E., Barba-Santos, M.G., Vega-Zepeda, A., Collado-Vides, L., 2017. Severe impacts of brown tides caused by Sargassum spp. on near-shore Caribbean seagrass communities. Mar. Pollut. Bull. 122, 272–281. https://doi.org/10.1016/j.marpolbul.2017.06.057.
Wang, M., Hu, C., 2016. Mapping and quantifying Sargassum distribution and coverage in the Central West Atlantic using MODIS observations. Remote Sens. Environ. 183, 350–367. https://doi.org/10.1016/j.rse.2016.04.019.
Wang, M., Hu, C., Barnes, B.B., Mitchum, G., Lapointe, B., Montoya, J.P., 2019. The great Atlantic *Sargassum* belt. Science 365, 83–87. https://doi.org/10.1126/science.aaw7912.
Wei, T., Simko, V., 2021. R package 'corrplot': Visualization of a Correlation Matrix (Version 0.92). https://github.com/taiyun/corrplot.
World Meteorological Organization, 2024. WMO confirms that 2023 smashes global temperature record. https://wmo.int/news/media-centre/wmo-confirms-2023-smashes-global-temperature-record.